NAVAL POSTGRADUATE SCHOOL
Monterey, California

DTIC
ELECTE
DEC 1 4 1988
S   D
H

THESIS

Development of a Compact Apparatus for
Determining Complex Parameters of Fluid-Filled
Porous Solids by Impedance Techniques

by

Steven D. Grant

September 1988

Thesis Advisor:	S. R. Baker
Co-Advisor	O. B. Wilson

88 12 14

Security Classification of this page

REPORT DOCUMENTATION PAGE

1a Report Security Classification UNCLASSIFIED		1b Restrictive Markings			
2a Security Classification Authority		3 Distribution Availability of Report			
2b Declassification/Downgrading Schedule		Approved for public release; distribution is unlimited.			
4 Performing Organization Report Number(s)		5 Monitoring Organization Report Number(s)			
6a Name of Performing Organization Naval Postgraduate School	6b Office Symbol *(If Applicable)* 3A	7a Name of Monitoring Organization Naval Postgraduate School			
6c Address *(city, state, and ZIP code)* Monterey, CA 93943-5000		7b Address *(city, state, and ZIP code)* Monterey, CA 93943-5000			
8a Name of Funding/Sponsoring Organization	8b Office Symbol *(If Applicable)*	9 Procurement Instrument Identification Number			
8c Address *(city, state, and ZIP code)*		10 Source of Funding Numbers			
		Program Element Number	Project No	Task No	Work Unit Accession No

11 Title *(Include Security Classification)* DEVELOPMENT OF A COMPACT APPARATUS FOR DETERMINING COMPLEX PARAMETERS OF FLUID-FILLED POROUS SOLIDS BY IMPEDANCE TECHNIQUES

12 Personal Author(s) Grant, Steven D.			
13a Type of Report Master's Thesis	13b Time Covered From To	14 Date of Report *(year, month, day)* 1988 September	15 Page Count 74

16 Supplementary Notation The views expressed in this thesis are those of the author and do not reflect the official policy or position of the Department of Defense or the U.S. Government.

17 Cosati Codes			18 Subject Terms *(continue on reverse if necessary and identify by block number)*
Field	Group	Subgroup	Bulk Modulus, Acoustic Impedance, Acoustic Coupler, Complex Mass Density,
			Fluid Saturated . (high)

19 Abstract *(continue on reverse if necessary and identify by block number)* ρ

A method for determining the complex bulk modulus B and the complex mass density ρ of a fluid contained in a rigid porous solid is investigated. The fluid filled solid is contained within a small cylindrical cavity capped on each end by identical transducers. This method, suitable for an acoustically "soft" transducer, is based upon electroacoustic network theory. B and ρ are obtained from the input electrical impedance of each transducer when they are wired in parallel "in-phase" and "out-of-phase", respectively. A description of the apparatus and preliminary experimental results are presented. *Thesis*,

20 Distribution/Availability of Abstract			21 Abstract Security Classification
[X] unclassified/unlimited	[ ] same as report	[ ] DTIC users	UNCLASSIFIED
UNCLASSIFIED			
22a Name of Responsible Individual PROF. S. R. Baker		22b Telephone *(Include Area code)* (408) 646-2729	22c Office Symbol 61BA

DD FORM 1473, 84 MAR	83 APR edition may be used until exhausted	security classification of this page
	All other editions are obsolete	UNCLASSIFIED

i

**Development of a Compact Apparatus for Determining Complex
Parameters of Fluid-Filled Porous Solids by Impedance Techniques**

by

Steven D. Grant
Lieutenant, United States Navy
B. S., United States Naval Academy, 1979

Submitted in partial fulfillment of the
requirements for the degrees of

MASTER OF SCIENCE IN ENGINEERING ACOUSTICS

and

MASTER OF SCIENCE IN SYSTEMS TECHNOLOGY

(Antisubmarine Warfare)

from the

NAVAL POSTGRADUATE SCHOOL
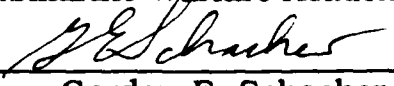
September 1988

Author: _____
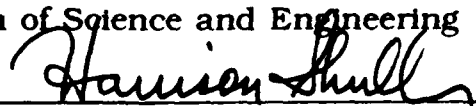Steven D. Grant

Approved by: _____
Steven R. Baker, Co-Advisor

_____
Oscar B. Wilson, Co-Advisor

_____
Anthony A. Atchley, Chairman
Engineering Acoustics Academic Committee

_____
Robert N. Forrest, Chairman
Antisubmarine Warfare Academic Group

_____
Gordon E. Schacher
Dean of Science and Engineering

_____
Harrison Shull
Academic Dean

ii

ABSTRACT

A method for determining the complex bulk modulus $\tilde{B}$ and the complex mass density $\tilde{\rho}$ of a fluid contained in a rigid porous solid is investigated. The fluid filled solid is contained within a small cylindrical cavity capped on each end by identical transducers. This method, suitable for an acoustically "soft" transducer, is based upon electroacoustic network theory. $\tilde{B}$ and $\tilde{\rho}$ are obtained from the input electrical impedance of each transducer when they are wired in parallel "in-phase" and "out-of-phase", respectively. A description of the apparatus and preliminary experimental results are presented.

Accession For		
NTIS GRA&I	☑	
DTIC TAB	☐	
Unannounced	☐	
Justification		
By		
Distribution/		
Availability Codes		
	Avail and/or	
Dist	Special	
A-1		

iii

TABLE OF CONTENTS

ACKNOWLEDGEMENTS

I. **INTRODUCTION**

Geoacoustic models of fluid-saturated sediment contain several parameters which depend on the microscopic pore geometry of the sediment [Ref. 1, Ref. 2, Ref. 3]. These parameters are very difficult to determine from the usual measurements of dilatational sound speed and attenuation. In particular, the parameters which determine what is essentially the complex effective mass density $(\tilde{\rho})$ of the fluid contained in the pores are among the least well known [Ref. 4, Ref. 5]. For this reason it would be very desirable to directly measure the complex effective fluid mass density and thereby extract these parameters for various typical microscopic pore geometries. To date, direct measurements of $\tilde{\rho}$ have been conducted with helium filled sintered bronze samples [Ref. 6].

A method is proposed for measuring the complex effective mass density of a fluid contained in a rigid porous solid. The fluid-filled solid is contained in a cylindrical cavity capped on both ends by identical transducers. The method investigated is an impedance method based upon electroacoustic network theory. This method may also be used to measure the complex bulk modulus $(\tilde{B})$, and thereby obtain the complex speed of sound, using only a small sample. The impedance method is suitable for use with acoustically "soft" transducers at the ends of the sample chamber. Moving coil, high-fidelity tweeters were used in this investigation. $\tilde{B}$ and $\tilde{\rho}$ are obtained from the input electrical impedance of the transducers, which is

1

related to the acoustic impedance presented to each face, when they are wired in parallel "in-phase" and "out-of-phase", respectively. If the two transducers are identical in electrical, mechanical, and acoustical characteristics, data reduction is remarkably simplified.

The objectives of this research are to (1) identify and characterize two identical, acoustically "soft" transducers; (2) develop a compact apparatus to measure both $\tilde{B}$ and $\tilde{\rho}$; and (3) validate the technique using samples for which the desired values are known or easily calculated.

2

II. __THEORY__

A. __INTRODUCTION__

In this chapter the network equations from which $\tilde{B}$ and $\tilde{\rho}$ can be extracted are developed from the input electrical impedance of the transducers. This development is presented in three major sections. In the first section the network theory associated with the acoustics of the chamber is presented. This development is general in form but is simplified by use of the long wavelength approximation. The specific case of matched transducers is then analyzed, resulting in a simple expression for the acoustic impedance presented to the face of each transducer.

In the second section the network theory for the transducers selected for the experiment is presented. The relationships between the electrical and mechanical parameters are developed. These parameters are then modeled in an equivalent electrical circuit. The third and final section consolidates the acoustic network of the chamber and the electroacoustic network of the drivers. After this consolidation is accomplished, circuit theory is then used to derive $\tilde{B}$ and $\tilde{\rho}$ from the measured input electrical impedance.

B. __ACOUSTIC IMPEDANCE IN SAMPLE CAVITY__

1. __Initial Development__

The goal of this section is to demonstrate how the two complex parameters $\tilde{B}$ and $\tilde{\rho}$ can be extracted from the acoustic impedance

presented to the face of the transducers on each end of a fluid-filled porous sample in a cavity. A simple diagram to aid in explaining this is shown in Figure 1.
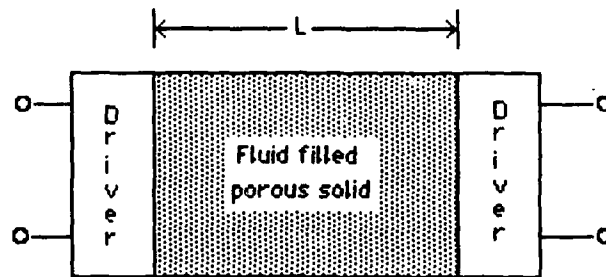
Figure 1. Simple Chamber.

In this figure, there are two transducers, or drivers, facing one another with the sample in between. The cross-sectional area of the drivers are assumed to be equal to the cross-sectional area of the chamber. The two port network representing the acoustic properties of this chamber is shown in Figure 2.
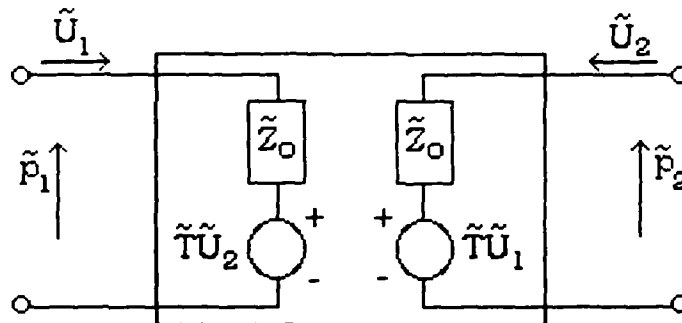
Figure 2. Acoustic Two Port Network.

In Figure 2, all the parameters listed are, in general, complex. A complex parameter is represented with a tilda (~) over the symbol.

4

The symbols are defined as:

$\tilde{p}$ = the acoustic pressure at the face of the transducer.

$\tilde{U}$ = the volume velocity produced by the transducer.

$\tilde{Z}_0$ = the acoustic impedance seen by a transducer when the other transducer is held fixed, or blocked.

$\tilde{T}$= the transfer impedance between the two transducers.

The appearance of $\tilde{Z}_0$ and $\tilde{T}$ in each branch of the network is a consequence of the reciprocal property of the acoustic field and the symmetry of the chamber. Expressions for $\tilde{Z}_0$ and $\tilde{T}$ for can be extracted when the appropriate boundary conditions and wave functions are applied, as described below. The subscripts 1 and 2 in Figure 2 associate the parameter with its respective driver.

2. Blocked Acoustic Impedance

The acoustic pressure and volume velocity can be obtained using the concept of a velocity potential ($\tilde{\Phi}$). If the velocity potential is known, the acoustic pressure ($\tilde{p}$) and particle velocity ($\vec{\tilde{u}}$) are derived using the following relationships [Ref. 7:pp. 104-106]

$$\vec{\tilde{u}} = \nabla \tilde{\Phi} , \qquad (2.1)$$

$$\tilde{p} = -\rho_0 \frac{\partial \tilde{\Phi}}{\partial t} , \text{ where } \rho_0 \text{ is bulk density.} \qquad (2.2)$$

As an example, for a time harmonic, sinusoidal wave in one dimension ($\vec{\tilde{u}}$ can now be expressed as $\tilde{u}$) of the form $e^{j(\omega t - kx)}$, these expressions reduce to

$$\tilde{u} = -jk\,\Phi_0\; e^{j(\omega t - kx)} , \qquad (2.3)$$

and $$\tilde{p} = -j\omega\rho_0\Phi_0\; e^{j(\omega t - kx)} . \qquad (2.4)$$

5

In Equations 2.3 and 2.4, Φ_0 is the magnitude of the velocity potential, $\tilde{u}$ is the velocity of the radiating face, ω is the angular frequency and k is the wave number.

Recall $\tilde{Z}_0$ is the acoustic impedance seen by a transducer when the other transducer is blocked. Figure 3 represents pictorially this condition (for ease of analysis, x=0 is referenced to the face of the blocked driver and the analysis performed for the left driver). The boundary condition at x=0 requires the velocity there to be zero.
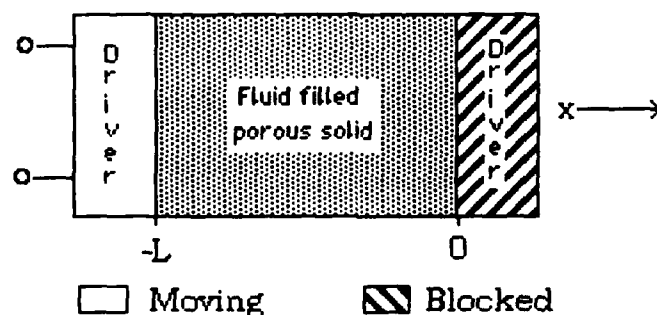
Figure 3. Blocked Acoustic Impedance.

Applying this condition results in the following forms for the velocity potential, acoustic pressure and particle speed (the periodic time dependence is suppressed):

$$\Phi = \Phi_0 \cos(kx). \qquad (2.5)$$

$$\tilde{p} = -j\omega\rho_0\Phi_0 \cos(kx). \qquad (2.6)$$

$$\tilde{u} = -k\Phi_0 \sin(kx). \qquad (2.7)$$

At x= -L these become:

$$\Phi = \Phi_0 \cos(kL). \qquad (2.8)$$

$$\tilde{p} = -j\omega\rho_0\Phi_0 \cos(kL). \qquad (2.9)$$

$$\tilde{u} = k\Phi_0 \sin(kL). \qquad (2.10)$$

6

For the transducer at x=-L,

$$\tilde{Z}_0 = \frac{\tilde{P}}{\tilde{U}} = \frac{\tilde{P}}{\tilde{u}\, S}, \qquad\qquad (2.11)$$

where S is the cross sectional area of the transducer face. Substituting Equations 2.9 and 2.10 into Equation 2.11 gives

$$\tilde{Z}_0 = \frac{-j\omega\, \rho_0 \Phi_0 \cos(kL)}{S\, k\, \Phi_0 \sin(kL)}. \qquad\qquad (2.12)$$

Using the relationship $kc=\omega$ yields

$$\tilde{Z}_0 = \frac{-j\,\rho_0\, c}{S}\, \cot(kL). \qquad\qquad (2.13)$$

This expression for $\tilde{Z}_0$ will be simplified later when the long wavelength approximation is applied.

3. Transfer Impedance

$\tilde{T}$ is a transfer impedance and is the ratio of the pressure on the face of a blocked transducer at one end of the chamber to the volume velocity of a moving transducer at the other end (again, x=0 is referenced to the blocked transducer and analysis performed on the left driver). Figure 4 below represents this situation.
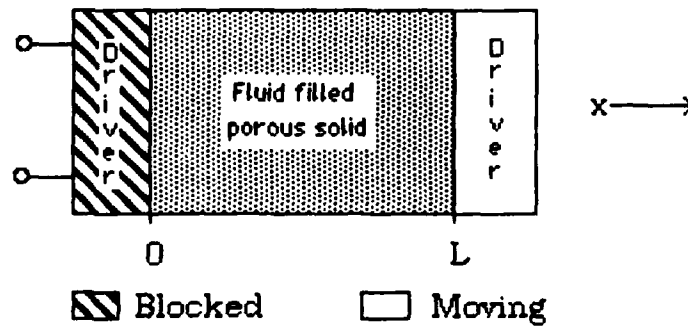
Figure 4. Transfer Impedance.

The boundary condition at x=0 requires the velocity there to be zero. Applying this condition results in the forms expressed in Equations 2.5 through 2.7. Pressure at x=0 and the particle velocity at x=L can then be expressed as

$$\tilde{p}(0) = -j\omega \rho_0 \Phi_0 \ , \tag{2.14}$$

and

$$\tilde{u}(L) = -k \Phi_0 \sin(kL) \ . \tag{2.15}$$

By inspection of Figure 2, note $U_2 = -S\, u(L)$, so that

$$\tilde{T} \equiv \frac{\tilde{p}(0)}{\tilde{U}_2} = \frac{\tilde{p}(0)}{-S\,\tilde{u}(L)}. \tag{2.16}$$

Substituting Equations 2.14 and 2.15 into Equation 2.16 yields

$$\tilde{T} = \frac{-j\omega\,\rho_0\,\Phi_0}{S\,k\,\Phi_0\,\sin(kL)} \ . \tag{2.17}$$

This can further be simplified to the following expression:

$$\tilde{T} = \frac{-j\,\rho_0 c}{S\,\sin(kL)} \ . \tag{2.18}$$

The long wavelength approximation will now be applied to $\tilde{Z}_0$ and $\tilde{T}$.

4. Long Wavelength Approximation

This experiment will be conducted at frequencies for which the wavelength is much larger than the size of the cavity. The sine and cosine terms are expanded in Taylor series form, and since the product (kL) is small, the terms of fourth order and higher are negligible. The sine and cosine functions are expressed as:

$$\sin(kL) \cong kL - \frac{(kL)^3}{3!} \ . \tag{2.19}$$

$$\cos(kL) \cong 1 - \frac{(kL)^2}{2!} \ . \tag{2.20}$$

8

Applying these approximations to Equation 2.13 give

$$\tilde{Z}_0 = \frac{-j \rho_0 c}{S} \cot(kL) \cong \frac{-j\omega\rho_0}{S k^2 L} \left[\frac{1 - \frac{(kL)^2}{2}}{1 - \frac{(kL)^2}{6}} \right]. \quad (2.21)$$

Using a Taylor expansion on the denominator i.e.,

$$\left[1 - \frac{(kL)^2}{6} \right]^{-1} \approx 1 + \frac{(kL)^2}{6}, \quad (2.21a)$$

the above equation is reduced to Equation 2.22:

$$\tilde{Z}_0 \cong \frac{-j\rho_0 c}{S} \left[\frac{1 - \frac{(kL)^2}{3}}{kL} \right]. \quad (2.22)$$

Recalling $\omega = kc$ and B (bulk modulus) $= \rho c^2$,

$$\tilde{Z}_0 \cong \frac{B}{j\omega SL} + \frac{j\omega\rho L}{3S}. \quad (2.23)$$

Similar relationships are applied to the expression for $\tilde{T}$ found in Equation 2.18, resulting in:

$$\tilde{T} \cong \frac{B}{j\omega SL} - \frac{j\omega\rho L}{6S}. \quad (2.24)$$

With these expressions, the acoustic impedance presented to the face of each transducer can now be determined. The next step is to apply these equations to the case when the two transducers are identically driven in-phase and out-of-phase.

9

5. Identical Transducers

When matched transducers are used in the cavity and are driven identically either in-phase or out-of-phase, a solution for the acoustic impedance $(\tilde{Z}_{ac})$ presented to each transducer face is readily obtained. Consider Figure 2. Using this figure, the acoustic pressure at the face for each transducer can be expressed as:

$$\tilde{p}_1 = \tilde{Z}_0 \tilde{U}_1 + \tilde{T} \tilde{U}_2 . \qquad (2.25)$$

$$\tilde{p}_2 = \tilde{T} \tilde{U}_1 + \tilde{Z}_0 \tilde{U}_2 . \qquad (2.26)$$

If the transducers are identical and driven in phase, $\tilde{U}_1 = \tilde{U}_2 \equiv \tilde{U}$. Equations 2.21 and 2.22 become:

$$\tilde{p}_1 = \tilde{Z}_0 \tilde{U} + \tilde{T} \tilde{U} \equiv \tilde{p}. \qquad (2.27)$$

$$\tilde{p}_2 = \tilde{T} \tilde{U} + \tilde{Z}_0 \tilde{U} \equiv \tilde{p}. \qquad (2.28)$$

Selecting either equation, and solving for the ratio of acoustic pressure to *volume velocity* gives

$$\tilde{Z}_{ac} = \tilde{Z}_0 + \tilde{T} , \qquad (2.29)$$

where $\tilde{Z}_{ac}$ is the acoustic impedance. Substituting Equations 2.23 and 2.24 into the above gives

$$\tilde{Z}_{ac} \cong \frac{B}{j\omega S(L/2)} . \qquad (2.30)$$

This is the same as for a closed cavity of length L/2. In this case, a pressure antinode exists at the midplane of the cavity.

If the same identical drivers are driven out of phase, the same approach is taken and the result is:

$$\tilde{Z}_{ac} \cong \frac{j\omega \rho (L/2)}{S} . \qquad (2.31)$$

This is the same as for an open cavity of length L/2 (neglecting radiation). In this case, a pressure node exists at the midplane of the cavity.

6. Fluid-Filled Porous Solid

Equations have been derived for the acoustic impedance of a chamber filled only with fluid. When sound propagates in a fluid-filled, rigid porous body, acoustic energy losses occur due to the thermal conductivity and shear viscosity of the fluid. Consequently, the bulk modulus and effective mass density become complex. Equations 2.30 and 2.31 now become:

$$\tilde{Z}_{ac} \cong \frac{\tilde{B}}{j\omega PS(L/2)} \text{, and} \qquad (2.32)$$

$$\tilde{Z}_{ac} \cong \frac{j\omega(L/2)}{PS}\tilde{\rho} . \qquad (2.33)$$

The additional parameter, P, is the porosity. The porosity is defined as the ratio of the volume occupied by the fluid to the total sample volume. It is required since the cross sectional area for fluid interaction is reduced by the frame of the porous material. A formal derivation of the porous media effects is presented in the Appendix.

C. TRANSDUCERS

Since this research involves determining complex mechanical quantities from electrical impedance measurements, it is important to first identify the impedance of the transducers used. The transducers used are antireciprocal, moving coil type. The theory for this type of transducer is well understood [Ref. 8].

11

Equations have been developed to explain the relationships between voltage applied to a transducer and the force on its radiating face. The equations are:

$$\tilde{V} = \tilde{Z}_{EB}\, \tilde{I} + (Bl)\, \tilde{u}, \qquad (2.34)$$

$$\tilde{F} = -(Bl)\, \tilde{I} + \tilde{Z}_{mo}\, \tilde{u}. \qquad (2.35)$$

In the above equations:

$\tilde{V}$ = the voltage across the input of the transducer.

$\tilde{I}$ = the input current to the transducer.

$\tilde{F}$ = the force on the radiating surface.

$\tilde{u}$ = the velocity of the radiating surface.

$\tilde{Z}_{EB}$ = the blocked electrical impedance ($\tilde{V}/\tilde{I}$; $\tilde{u}$=0).

$\tilde{Z}_{mo}$ = the open circuit mechanical impedance ($\tilde{F}/\tilde{u}$; $\tilde{I}$=0).

(Bl) = the product of the magnetic field and length of coil in the gap of the driver = Transduction coefficient.

The moving coil transducer can further be modeled by a simple equivalent electrical circuit (in the mobility analog) given in Figure 5 [Ref. 7:p. 352]:
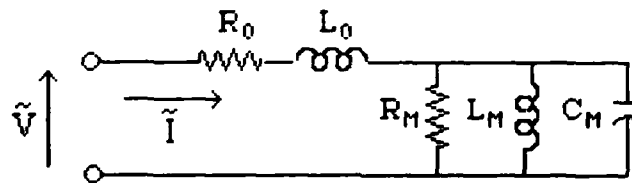
Figure 5. Driver Equivalent Circuit.

In the figure above,

R_0 = Blocked electrical resistance,

L_0 = Blocked electrical inductance,

R_M = Electrical equivalent mechanical resistance,

12

L_M = Electrical equivalent mechanical inductance,

C_M = Electrical equivalent mechanical capacitance.

The electrical equivalents are obtained from the following relationships [Ref. 9]:

$$R_M = \frac{(Bl)^2}{R_{mech}} . \tag{2.36}$$

$$L_M = \frac{(Bl)^2}{k} . \tag{2.37}$$

$$C_M = \frac{m}{(Bl)^2} . \tag{2.38}$$

The parameters R_{mech}, k and m are the mechanical resistance, stiffness and mass of the driver, respectively. From the above relationships, if the stiffness, moving mass, mechanical resistance, transduction coefficient and blocked electrical impedance are known, the electrical impedance of the driver as a function of frequency can be predicted.

Additionally, for the transducers selected, there is an extra stiffness existing due to the air in the cavity behind the dome of the voice coil. This stiffness should exhibit the characteristics of an acoustic cavity [Ref. 10] given by,

$$k = \frac{\gamma S^2 P_o}{V} , \tag{2.39}$$

where

γ = ratio of the constant pressure to constant volume specific heat capacity for a gas,

S = the area of the driving face,

P_O = the ambient pressure,

V = the cavity volume.

This added stiffness modifies the equivalent electrical circuit presented in Figure 5. The modified circuit is illustrated in Figure 6. The new inductance, L_C , accounts for the additional dynamic stiffness. Note this model does not reflect any acoustic loading on the transducer. The effects of acoustic loading on the electrical properties of the transducers will be presented in the next section of this chapter.
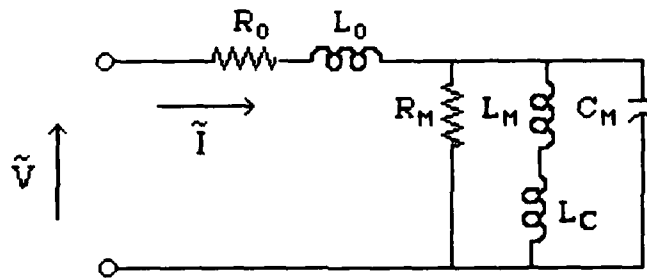
Figure 6. Modified Driver Equivalent Circuit.

D. COUPLER-DRIVER SYSTEM

When the electrical and mechanical characteristics of the two drivers are combined with the acoustical characteristics of the chamber, the two port system is given in Figure 7. In the figure below, the $\tilde{Z}_R$ are the electrical equivalent impedances of the radiation impedances presented to the transducers. The radiation impedance as used here is a mechanical impedance, i.e., a ratio of force to

14
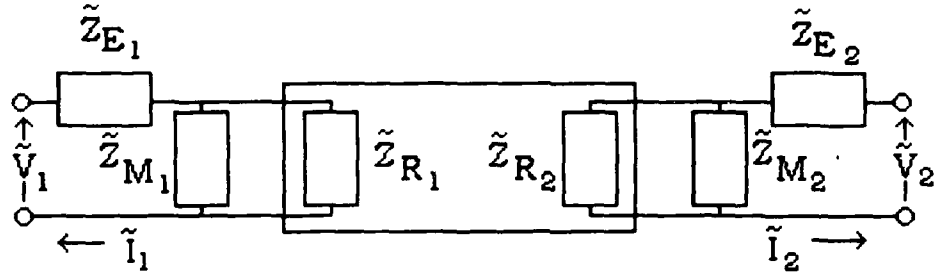
Figure 7. Combined Electrical Circuit.

velocity. This differs from the acoustic impedance by a factor of S^2, where S is the moving area of the driver.

When the drivers are driven identically in parallel "in-phase" or "out-of-phase", Figure 7 reduces to the equivalent circuit in Figure 8, where $\tilde{I}/2$ is the current to flow through each driver and $\tilde{V}$ is their common voltage.
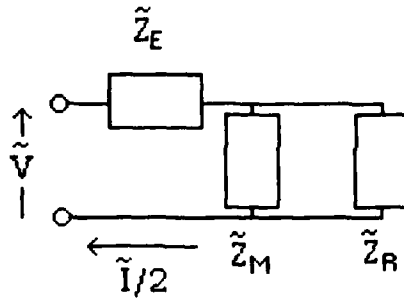
Figure 8. Combined Electrical Circuit For Identical Drivers.

Therefore, by measuring the input electrical impedance of the parallel combination $(\tilde{V}/\tilde{I})$, and knowing $\tilde{Z}_E$ and $\tilde{Z}_M$, $\tilde{Z}_R$ can be determined, and from it, the value of $\tilde{Z}_{ac}$ extracted according to:

$$\tilde{Z}_{in} \equiv \frac{\tilde{V}}{\tilde{I}} = \frac{1}{2}\left(\tilde{Z}_E + \frac{\tilde{Z}_M \tilde{Z}_R}{\tilde{Z}_M + \tilde{Z}_R}\right). \qquad (2.40)$$

15

Defining $\quad \tilde{Z} \equiv 2\,\tilde{Z}_{IN} - \tilde{Z}_E = \dfrac{\tilde{Z}_M\,\tilde{Z}_R}{\tilde{Z}_M + \tilde{Z}_R}\,,$ (2.41)

then $\quad \tilde{Z}_R = \dfrac{\tilde{Z}_M\,\tilde{Z}}{\tilde{Z}_M - \tilde{Z}}\,.$ (2.42)

The acoustic impedance is extracted from $\tilde{Z}_R$ in the mobility analog by,

$$\tilde{Z}_{ac} = \dfrac{(Bl)^2\,S^2}{\tilde{Z}_R}\,.$$ (2.43)

Once $\tilde{Z}_{ac}$ is determined, the complex bulk modulus is extracted using Equation 2.32 when the drivers are in-phase:

$$\tilde{B} = j\omega \left(\dfrac{L}{2}\right) PS\,\tilde{Z}_{ac}\,,$$ (2.44)

or the complex mass density using Equation 2.33 when out-of-phase:

$$\tilde{\rho} = \dfrac{PS}{j\omega\,(L/2)}\,\tilde{Z}_{ac}\,.$$ (2.45)

In summary, by measuring the input electrical impedance of two identical drivers used as the end caps of a small cylindrical chamber, the complex parameters $\tilde{B}$ and $\tilde{\rho}$ of the fluid in a porous rigid material can be determined, provided the characteristics of the drivers are known.

III. TRANSDUCER CHARACTERIZATION AND COUPLER DESIGN

A. BACKGROUND

The experimental portion of this investigation was conducted in two major phases. The first phase involved the selection and characterization of two matched transducers. Since it was crucial to characterize the transducers as accurately as possible, several experiments were conducted, and where possible, alternative methods used to verify previous results.

The second major phase involved the design and construction of a test chamber (coupler). The coupler was used to hold the selected transducers and the test sample. Once this was completed, measurements were made to verify the use of the input electrical impedance to extract physical parameters.

In this chapter the experimental apparatus used in each phase is described. Accompanying the description is an explanation of how the apparatus functions. Finally, sample data are presented.

B. TRANSDUCER SELECTION AND PARAMETER CHARACTERIZATION

1. Matched Transducer Selection

Matched transducers can be obtained by either constructing the transducers from identical components or by obtaining many samples of a manufactured product and testing several units until two matched transducers are found. The latter method was selected, primarily due to the experience of Hofler [Ref. 11]. Hofler had worked with

17

acoustically "soft" (moving coil) transducers. The type of transducer he used would meet the requirements of this experiment.

The transducers are nominal one-inch diameter domed tweeters. They are manufactured by Philips, Model AD062T8 [Ref. 12]. The dome is made of a water-resistant polyvinyl material. The cover of the driver is easily removed. Once this is done, the voice coil and its support ring can be readily detached from the magnet. A cutaway view of the driver (minus cover) is provided in Figure 9.
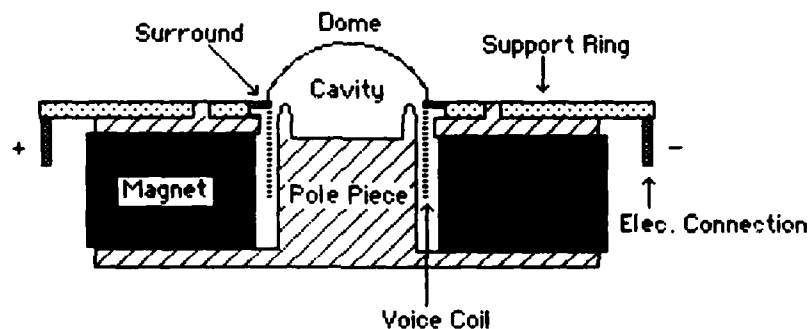
Figure 9. Cutaway View of Philips Driver.

Several drivers were obtained and the impedance as a function of frequency determined using a Hewlett-Packard Impedance Analyzer, Model 4194A (HP-4194A) [Ref. 13], as follows. The drivers were mounted on a large baffle and placed in an anechoic chamber. The resistive and reactive components of the impedance of each driver were measured over the frequency range from 100 Hz to 10 kHz. The impedance curves for each driver were then compared and two drivers with similar responses were selected for further testing.

18

Table 3.1 presents the resistance and reactance values of the two transducers selected at their respective mechanical resonance frequencies. The similarities in resonance values resulted in their selection for further experimentation.

TABLE 3.1. RESONANCE VALUES FOR SELECTED DRIVERS.			
Driver	Frequency (Hz)	Resistance(ohms)	Reactance (ohms)
1	954.0	65.19	1.36
2	954.0	70.31	4.36

2. Source Strength

To further confirm the similarity of the two drivers, the source strength of each was found. The source strength measurement is best explained by the use of Figure 10.

The HP-4194A provides the current for the driver. In the Gain-Phase mode, it is able to measure the voltage difference between a test and a reference channel, or display the voltage of each channel. In this case, the reference is the voltage associated with the current through a 10 ohm resistor on the return side of the driver. The HP-4194A was swept through the desired frequency span. The output was then printed on an accompanying printer and stored in the impedance analyzer for further analysis. The distance was measured from speaker to microphone for source strength calculations.

The calibration standard was a General Radio (GR) microphone. The calibration of this microphone was accomplished by use of a pistonphone. The calibration was further checked by using a less

19

accurate GR Calibrator. The sensitivity level obtained by these two methods was then verified against the calibration curves accompanying the microphone.
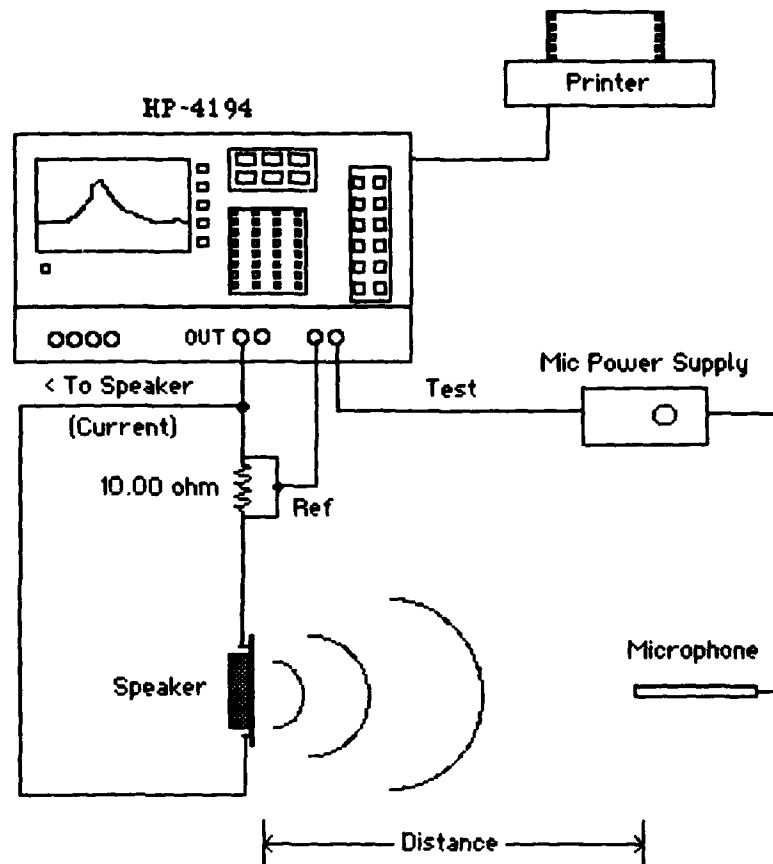
Figure 10. Source Strength Determination.

Sweeps were conducted for the two selected drivers. Printouts of the reference and test channels were obtained for each driver, and then compared. When the output from the two different drivers were compared, they were virtually identical. Based upon this, these

20

transducers were retained for the remaining portions of the experiment.

3. Transducer Parameter Determination

Five parameters must be known to adequately predict the performance of the moving coil transducers. These parameters are the blocked electrical impedance $(\tilde{Z}_{BE})$, driver stiffness (k), moving mass (m), the transduction coefficient (Bl) and mechanical resistance (R_m).

a. Electrical Parameters

The easiest electrical parameters to determine are the blocked electrical parameters. Two methods were employed to accomplish this. In the first method the voice coil was removed from the driver. With the coil removed, a digital multimeter was used to determine the direct current resistance of the coil. By use of a Hewlett-Packard Low Frequency Impedance Analyzer, Model 4192 (HP-4192), the inductance at several frequencies was measured and then averaged. The second method was similar to the first except the voice coil remained in the driver. The moving portion was held fast. Resistance and inductance were measured over several frequencies and averaged.

The impedance obtained by these two methods was used to determine the best value for comparing modeled to measured performance. Table 3.2 presents typical data obtained by these measurements.

21

The DC resistance did not vary appreciable from the in-magnet case to the out-of-magnet case. However, the blocked inductance changed by a factor of ten from the in-magnet to out-of-magnet case. The out-of-magnet value was selected for use since it provided the best fit to the modeled performance of the lumped parameters. The in-magnet inductances were difficult to obtain since it was a dynamic measurement and blocking the voice coil was not easy.

TABLE 3.2. BLOCKED ELECTRICAL PARAMETERS.		
Blocked Resistance (ohms)		Blocked Inductance (mH)
Coil Removed Driver		
1	6.544	0.11 (at 30 Hz)
2	6.542	0.11 (at 30 Hz)
Coil Installed Driver		
1	6.546	1.07 (at 30 Hz)
2	6.508	1.10 (at 30 Hz)

Since it was crucial to know the blocked impedance as accurately as possible, the diaphragm of a similar driver with identical out-of-magnet electrical parameters was rigidly clamped to the magnetic structure using epoxy resin. When the epoxy was cured, the blocked inductance was measured as a function of frequency. The results are presented in Figure 11. The data reveals the blocked inductance is frequency dependent. To properly account for this dependence, the blocked impedance over the desired frequency range will be obtained from the epoxied driver. The frequency dependent

22

blocked impedance data can then be stored in the data registers of the HP-4194A for later use when the acoustic impedance experiments are conducted.
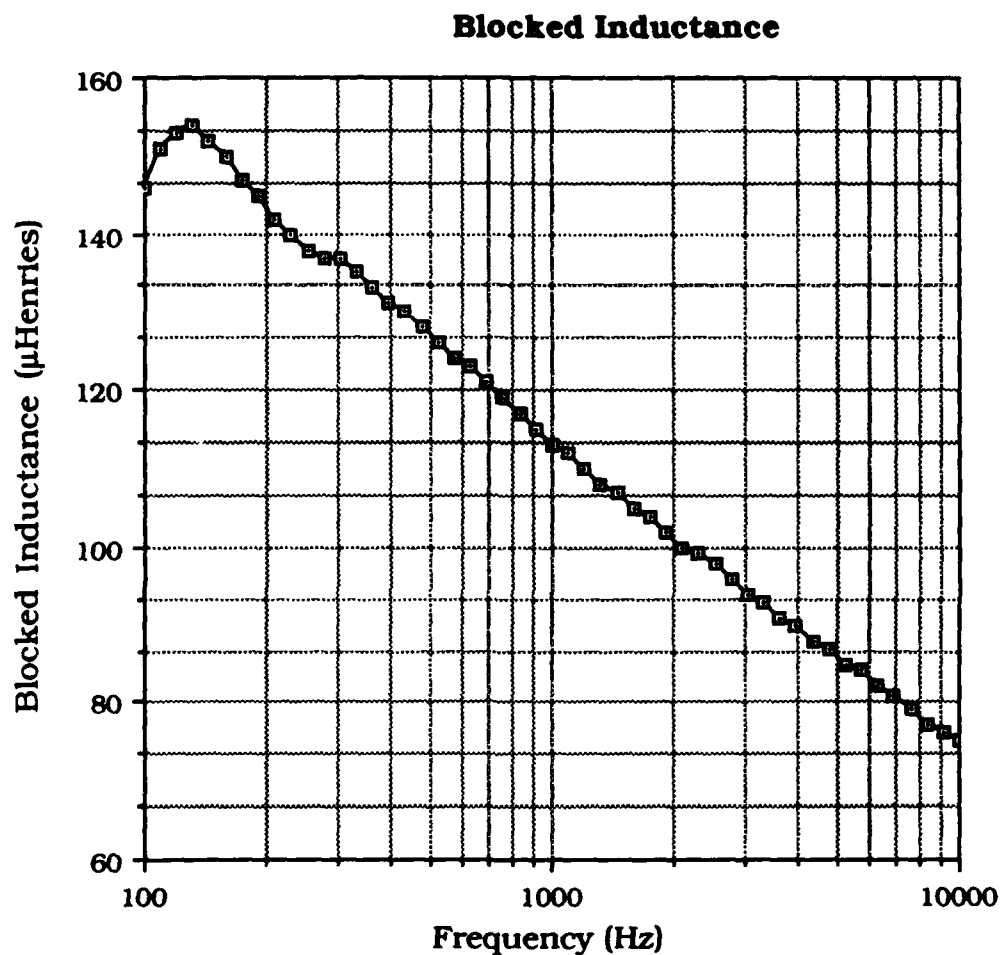
Blocked Inductance

Figure 11. Driver Blocked Inductance with Coil in the Magnetic Structure

b. Driver Stiffness

Several methods can be used to determine the stiffness of the transducers. The first method attempted was a static method.

23

The motivation for making a static determination is the ease of measurement. If a known mass Δm is added to the dome and the voice coil deflection Δx is measured, the stiffness can be determined by:

$$\Delta mg = k\Delta x. \qquad (3.1)$$

In the experiment performed, the voice coil deflection was measured with a linear variable differential transformer (LVDT). The LVDT operates with alternating current (ac) and has the property that the voltage across the secondary is linearly proportional to the position of the plunger. If the change in LVDT secondary voltage is measured and the LVDT calibrated, Equation 3.1 can be written as:

$$\Delta mg = k \, \Delta V \, \frac{dx}{dV} \, , \qquad (3.2)$$

where ΔV is the output voltage of the LVDT and dx/dV is the reciprocal of the slope of the curve (line) of output voltage versus displacement.

The LVDT used was manufactured by the Collins Corporation, Model LMS-119V22-01 [Ref. 14]. It was calibrated using a calibration stand and a micrometer. The calibration stand held the transformer securely in place while the transformer's lightweight plunger was allowed to rest atop the micrometer. As the micrometer position was changed, the output of the LVDT secondary was recorded. The data obtained were plotted as LVDT secondary output voltage versus micrometer position (Figure 12). The slope of this line represents the change in voltage for a change in position. Table 3.3 lists the slope and its relative uncertainty.

24

LVDT Calibration Curve
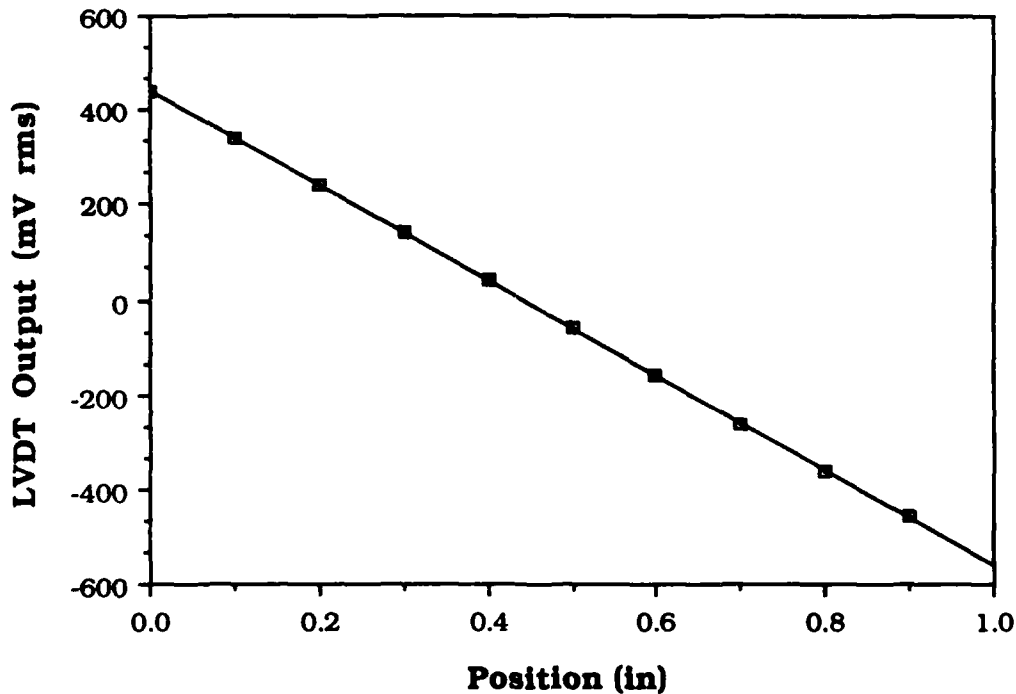
Figure 12. LVDT Calibration Curve.

TABLE 3.3. LVDT CALIBRATION.	
Slope [mV (rms) / in]	Relative Uncertainty (%)
-996.2	0.19

A special ring was machined from lightweight aluminum to fit smoothly around the voice coil dome. Ring shaped brass weights were added to the special ring. A 1000 Hz stabilized sine wave was applied to the primary side of the LVDT, whose plunger rested upon the top of the voice coil dome. The change in LVDT secondary voltage caused by the change in position due to the weight of the brass ring was measured using a Stanford Research Lock-in Analyzer, Model 530 [Ref. 15]. Table 3.4 lists the data points obtained using this method.

	Mass Added (g)	LVDT Output (mV)
	TABLE 3.4. STATIC STIFFNESS DATA.	
Driver 1	14.98	2.663
	41.80	6.751
	84.84	13.26
	109.90	17.45
Driver 2	14.98	2.693
	40.49	6.714
	84.84	14.52
	109.90	17.35

Two methods can be used to reduce the stiffness data. Both were utilized to provide a cross-check. The first involves plotting the change in LVDT secondary voltage as a function of mass added to the driver. The slope of this line is:

$$\text{Slope} = \frac{-g}{k} \frac{dV}{dx} . \qquad (3.3)$$

Solving for k:

$$k = \frac{-g}{\text{Slope}} \frac{dV}{dx} . \qquad (3.4)$$

The second method of reduction involves calculating k directly from each data point:

$$k = - \frac{\Delta mg}{\Delta V} \frac{dV}{dx} . \qquad (3.5)$$

These values for stiffness are then plotted versus the force applied. The result should be a nearly horizontal line whose intercept reflects the value of stiffness for small displacements.

Both schemes were employed to analyze the data. Due to a slight but observable nonlinearity in the results from the first method,

26

the second method was selected for final data reduction. The transducers are less stiff at low displacements and tend to be more stiff at high displacements. Since operation of the driver in the chamber experiment will be in the low displacement region, it was believed method two would provide a more realistic value for stiffness.

Table 3.5 lists the stiffness and relative uncertainty for each method of reduction. The difference due to the slight nonlinearity is seen by the difference in values.

TABLE 3.5 STIFFNESS OF SELECTED DRIVERS.		
Reduction Method	Stiffness (N/m)	Relative Uncertainty (%)
One		
Driver		
1	2448	1.6
2	2380	2.9
Two		
Driver		
1	2225	4.3
2	2118	4.4

Another way to determine stiffness is to extract it from the resonance frequency ($\omega=2\pi f$) and the (presumed known) moving mass:

$$\omega = \sqrt{\frac{k}{m}} \ . \qquad (3.6)$$

Since ω and m are known, this equation can be rearranged to solve for the stiffness, k:

$$k = m(2\pi f)^2 \ . \qquad (3.7)$$

This was the method finally selected because it eliminated a sizeable discrepancy that existed when the modeled electrical impedance of a driver was compared with its measured electrical impedance. As will

be discussed in the next section, the moving mass of an auxiliary driver was measured. Using this mass and the vacuum resonance frequency of each of the selected drivers, the stiffness for each selected driver was solved for and is listed in Table 3.6. The relative uncertainty is derived from the uncertainties of the moving mass and the resonance frequencies.

TABLE 3.6. STIFFNESS OF SELECTED DRIVERS		
Driver	Stiffness (N/m)	Relative Uncertainty (%)
1	5089	3.34
2	4687	3.34

c. Moving Mass

Several methods can be used to determine the moving mass of the transducers. The first is the method of added mass. With the driver operating in a vacuum, the resonance frequency is given by:

$$\omega = \sqrt{\frac{k}{m}} \ , \qquad\qquad (3.8)$$

where k is the stiffness constant and m the moving mass of the driver. If a mass m_i is added to the voice coil dome, the resonance frequency now becomes:

$$\omega_i = \sqrt{\frac{k}{m + m_i}} \ . \qquad\qquad (3.9)$$

By rearranging this formula, plotting the square of the period as a function of mass added, the slope of the line is $4\pi^2 / k$ and the intercept is $(4\pi^2 m) / k$. Dividing the intercept by the slope will yield the moving mass of the driver.

The method of using added masses to determine the moving mass of the driver was abandoned because of inconsistent results. This was due apparently in the inability to obtain satisfactorily stiff bonding of the added mass at frequencies of interest.

A second method is very simple. Assuming all the drivers are identical in construction, the mass of any given driver should equal that of another, within the tolerance of manufacturing. Using this assumption, an estimate of the moving mass can be obtained by measuring the mass of a diaphragm removed from an extra driver.

This was accomplished as follows. The diaphragm of an extra driver was cut away from the support ring. The surround was then removed from the diaphragm. The mass of each was measured separately, the results shown in Table 3.7.

TABLE 3.7 MOVING MASS OF SELECTED DRIVERS.	
Mass of Dome and Voice Coil(g)	Mass of Surround (g)
0.3086	0.0286

An initial estimate of the moving mass was taken as the mass of the voice coil and its diaphragm plus one-half the mass of the surround. The value was 0.2943 grams, with a relative uncertainty of 3 per cent based on half the mass of the surround. This value was later refined by curve fitting input electrical impedance data to an equivalent circuit model, described in Section II.C.

d. Transduction Coefficient

The transduction coefficient (Bl) is obtained directly as described below. The experimental setup is the same as the stiffness experiment. The two experiments are compatible and can be conducted together.

The driver was placed on a table facing up. A mass was added to the dome of the voice coil, resulting in a certain displacement of the diaphragm. A direct current was applied to the driver and adjusted to return the diaphragm to its original rest position, as indicated by the output voltage of a LVDT. By knowing the mass added, the applied force was calculated from F=mg. For this known force, the current required to exactly offset it was measured. Using the relationship F=mg=Bli, the Bl product was found. Several masses were added and the Bl product calculated for each. The Bl products were then averaged and the standard deviation calculated. Table 3.8 shows the data for Driver 1 obtained this way.

TABLE 3.8 TRANSDUCTION COEFFICIENT DATA.		
Mass Added (g)	Current (ma DC)	Transduction Coef. (T-m)
14.98	44.93	3.268
28.40	84.46	3.295
41.80	126.2	3.246
54.97	173.5	3.105
67.30	205.7	3.207
84.84	256.9	3.237
Average Transduction Coef. (T-m)		Relative Uncertainty (%)
3.226		2.0

30

A second method was used to check the values for the Bl product. Using the equation $F = Bli = -kx$, the derivative of this equation is taken with respect to current. This results in the expression:

$$Bl = -k\frac{dx}{dI}.$$ (3.10)

The stiffness (k) is obtained from by the procedure listed in Section III.B.3.b.

The term (dx/dI) is determined by applying a known direct current to the speaker and measuring the LVDT output. Table 3.9 lists sample data for Driver 1.

TABLE 3.9. CURRENT RESPONSE.	
Current (ma DC)	LVDT Output (mV)
-251.02	307.86
148.81	302.57
-93.79	299.47
56.26	297.19
-2.92	294.08
46.42	291.79
102.82	288.30
144.66	285.10
256.11	276.60

Linear regression was performed on the above data, with the current the independent variable, and the LVDT output voltage the dependent variable. The slope obtained by this linear regression is dV/dI. For Driver 1, the change in LVDT output with respect to direct current applied was 0.05609 mV/ma. Knowing this and the LVDT calibration,

31

$$\frac{dx}{dI} = \frac{dx}{dV} \frac{dV}{dI} . \qquad (3.11)$$

Applying Equation 3.5 to Equation 3.11, the result is:

$$Bl = -\frac{\Delta m \ g}{(\Delta V)} \frac{dV}{dI} . \qquad (3.12)$$

The transduction coefficient was calculated for each mass added, using the respective change in LVDT output. The output of the LVDT as a function of current applied was determined as discussed above. The Bl values were averaged and the standard deviation was used to calculate relative error. This resulted in the value of Bl listed in Table 3.10. The value is slightly higher than the one listed in Table 3.8. This was a result of the slight nonlinearity in stiffness. The first method used essentially a lower value of stiffness (displacement was always near zero). The second method incorporated a higher value of stiffness since the stiffness used was the slope of the force versus displacement for a wide variety of displacements. This slope was influenced by the increasing stiffness with increasing displacement, hence a higher transduction coefficient (displacement was over the range of driver motion).

TABLE 3.10 TRANSDUCTION COEFFICIENT OF DRIVER 1	
Transduction Coefficient (T-m)	Relative Uncertainty (%)
3.580	4.27

As a further check of Bl, a measurement of the B field in the gap was made with a Hall probe. The number of turns were counted

with a microscope and the length of wire estimated from this and the diameter of the voice coil. The result was a Bl product of 2.8 T-m. This aided in confirming the value of the transduction coefficient.

e. Mechanical Resistance

Mechanical resistance is obtained from measured values of electrical impedance near mechanical resonance. At resonance in vacuum, the magnitude of the impedance is approximately $R_O + R_M$ (the reactive component, $j\omega L_0$, was negligible) from the equivalent circuit, Figure 5. Using this fact, the mechanical resistance is obtained by rewriting Equation 2.36 in the form:

$$R_m = \frac{(Bl)^2}{|\tilde{Z}_{RES}| - R_O} \,. \tag{3.13}$$

Table 3.11 lists the resonance frequency, resonance impedance and resulting R_m for each of the drivers.

TABLE 3.11. VACUUM RESONANCE VALUES.			
Driver	Res. Freq. (Hz)	Impedance (ohms)	Mech Resistance (N-s/m)
1	662.00	63.11	0.1883
2	635.00	50.71	0.2172

f. Cavity Stiffness

From the cross section (Figure 9) view of the driver, one can observe a large cavity behind the dome of the speaker. This cavity provides significant additional stiffness to the system when operated in air. Since the drivers will be operated at various static pressures, the stiffness as a function of static pressure must be either known or eliminated.

33

An attempt to eliminate the stiffness of this cavity was tried first. A small hole was drilled through the pole piece of an auxiliary driver. The input electrical characteristics were measured for several different hole diameters. Instead of eliminating the stiffness, the driver now had additional loading caused by the air in the hole. This resulted in a coupled oscillator response which would only increase the complexity of the problem of added stiffness.

Since the cavity stiffness could not be eliminated, the next step was to determine the stiffness as a function of pressure. Assuming the cavity stiffness is due only to the gas in the cavity, it should be proportional to static pressure (see Equation 2.39). To determine the pressure dependence of the cavity stiffness, the driver was placed in a pressure chamber and the pressure was changed in controlled increments. Resonance frequency was recorded as a function of pressure. The resonance frequency dependence on the cavity stiffness is shown in Equation 3.14:

$$f^2 = \frac{k + k(p)}{(4\pi^2)(m + m_r)} ,$$
(3.14)

where:

f = measured resonance frequency.

k = static stiffness of the driver.

k(p) = the pressure dependent cavity stiffness.

m = moving mass of the driver.

m_r = radiation mass.

Table 3.12 lists the data obtained from this experiment using Driver 1.

TABLE 3.12. CAVITY STIFFNESS DATA.	
Pressure (in Hg)	Res. Frequency (Hz)
28.6	650.00
23.3	727.99
20.2	772.00
14.8	854.00
12.3	888.00
9.9	912.00
-0.51	1016.99

The square of the frequency was plotted as a function of pressure. The result was a straight line (the radiation mass, m_r, was negligible for the drivers at these frequencies). Once a linear relationship had been verified, the stiffness as a function pressure was solved for at each frequency. This stiffness was then plotted as a function of pressure. The result was another straight line, expressing cavity stiffness as a function of pressure. Figure 13 is a plot of these data. The equation of the line was solved for by regression, resulting in:

$$k(p) = \left(-159.4 + 0.07350 \, (P_0)\right) \frac{N}{m} \, . \qquad (3.15)$$

The relative error for a value from this equation is 3.9%. The intercept value for this equation was not forced to be zero. The negative value is a result of the random errors associated with this portion of the experiment.

To check the validity of Equation 3.15, the entire volume behind the dome of an auxiliary speaker was measured by filling it with a known volume of fluid. Using Equation 2.39, the stiffness was

calculated for a pressure equal to one atmosphere. The value agreed to within one percent of the value given by Equation 3.15.

g. Modeled Performance

Once all the electrical and mechanical parameters were identified for each driver, the parameters were converted to their equivalent electrical impedances using Equations 2.36 through 2.38. Utilizing a circuit analysis program, the impedance of the circuit in Figure 5 was modeled on a computer. The resulting modeled electrical impedance values were then compared to the actual
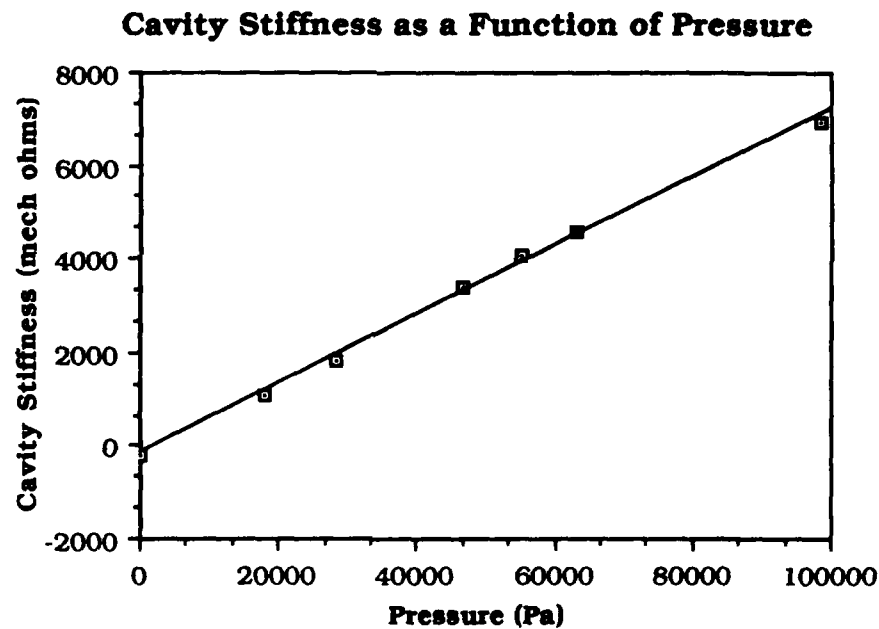

Figure 13. Cavity Stiffness Pressure Dependence.

electrical impedance measurements made earlier. The first model incorporated the electrical equivalent for stiffness obtained using added mass (Section III.B.3.b), and the electrical equivalent for mass extracted from resonance frequency (Equation 3.8). The results of

36

this model are given in Figure 14 (only the magnitude of the impedance is shown).

To resolve this discrepancy in the fit, the moving mass of an auxiliary transducer was measured and stiffness obtained from the resonance frequency (as described in Sections III.B.3.b and III.B.3.c). Figure 15 demonstrates the performance based upon the revised model. The fit has improved significantly.
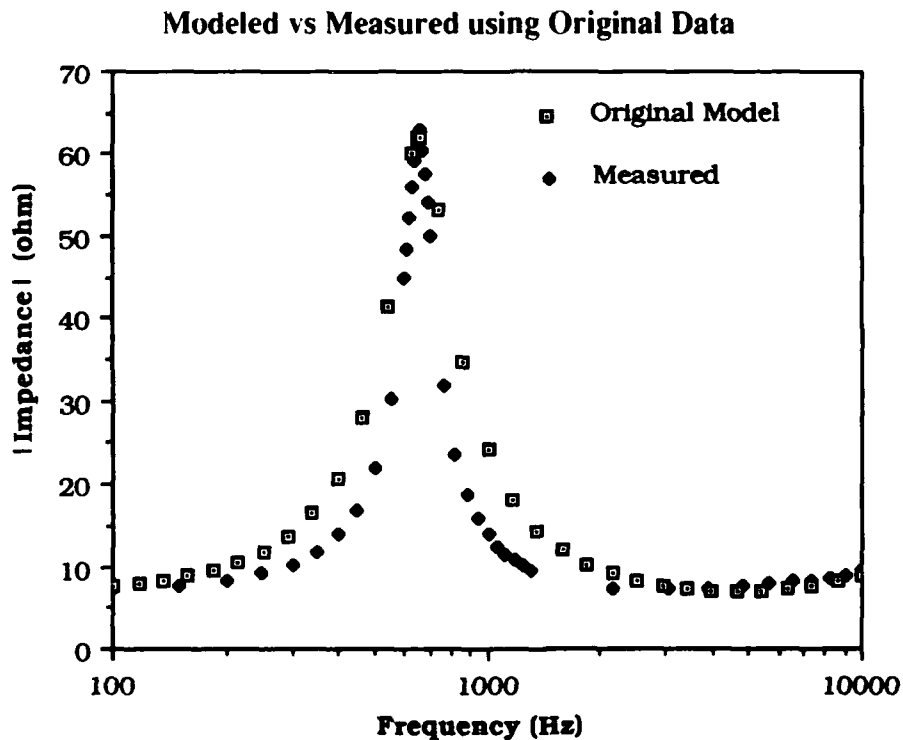

Figure 14. Modeled Performance With Original Mass Estimate.

A best fit was attempted using the built-in circuit analysis program of the HP-4194A. This further refined the values used in the model which will be used to extract the acoustic impedance from the input electrical impedance. Figure 16 demonstrates the excellent fit

37

of measured versus modeled. A best fit was performed for each driver. The values were then averaged to define a single transducer whose characteristics would be used for the "identical transducers". Table 3.13 lists the specific parameters and their electrical equivalents to be used in the circuit model (Figure 6) to extract the value of acoustic impedance.
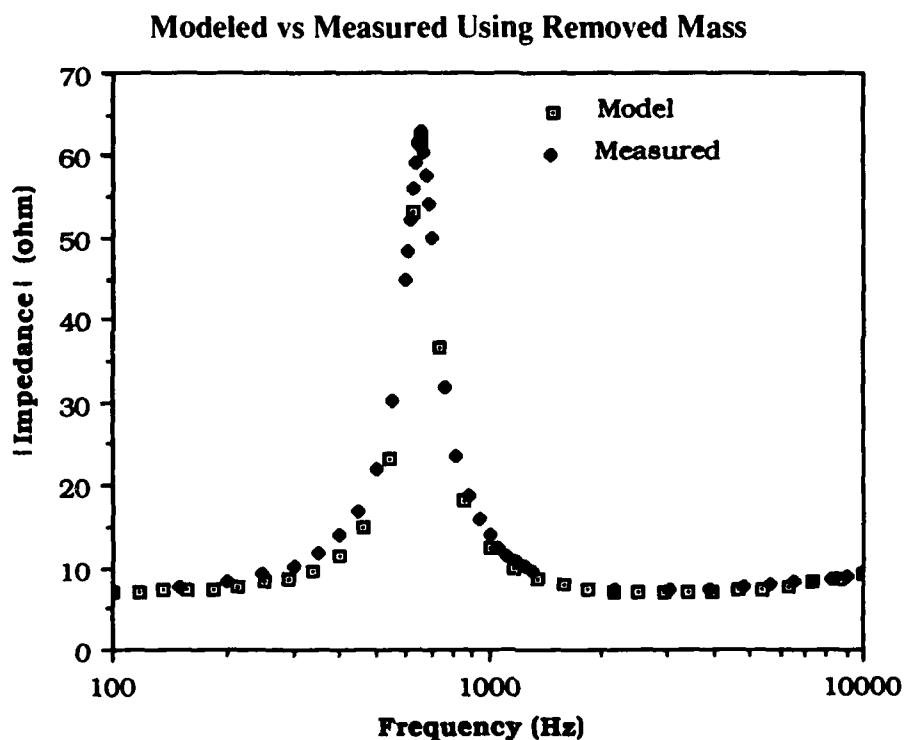
Modeled vs Measured Using Removed Mass

Figure 15. Modeled Performance With Removed Mass Estimate.

TABLE 3.13. MODEL TRANSDUCER PARAMETERS		
Parameter	Value	Units
Blocked Resistance	6.3521	ohms
Blocked Inductance	0.11	mH
Mechanical Resistance	49.08	ohms
Driver Mass	26.65	μF
Driver Stiffness	2.269	mH
Cavity Stiffness	1.351	mH

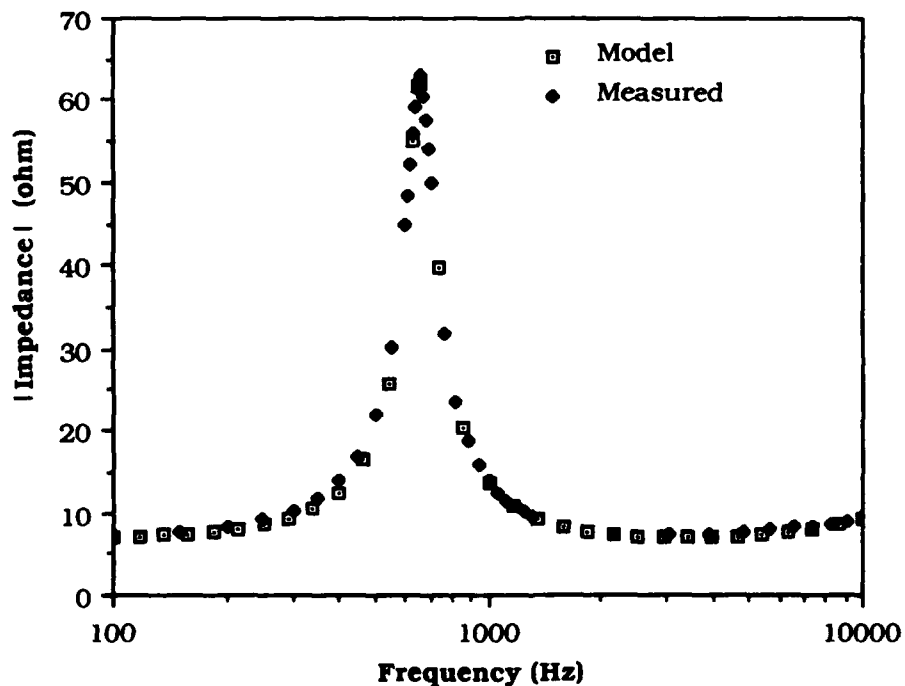**Modeled vs Measured for Revised Circuit Elements**

Figure 16. Best Fit Model.

C. COUPLER DESIGN AND CONSTRUCTION

1. Coupler Construction

Figure 17 is a cutaway view of the assembled cylindrical brass coupler (for clarity, only some dimensions are shown). The main parts of the coupler are the center chamber with sample sleeve and

39

two hermetically sealed driver chambers, one on each end. The drivers are secured in their respective chambers with a backing plate.

The dimensions of the coupler were dictated in part by the dimensions of the driver and by the size of tubing available for the sample sleeves. The inner diameter of the sample sleeving used had to be slightly greater than the driving face of the transducer. Once a sleeving size was selected, the sample chamber size was based upon the outer diameter of the sleeving. The length of the chamber was chosen to avoid finite wavelength effects for frequencies as high as one kilohertz.
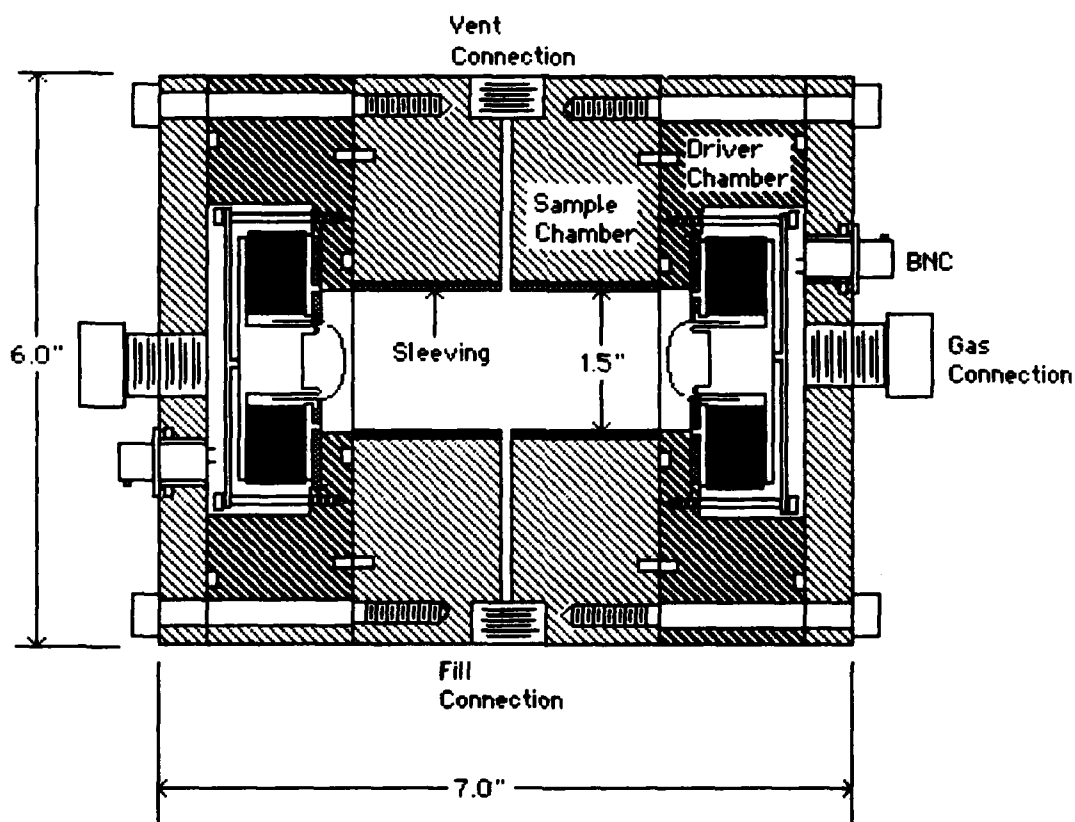

Figure 17. Cutaway View of Complete Coupler.

The sample chamber and the driver chambers are joined together and kept aligned via alignment pins. The entire coupler can be pressurized. The pressure in the sample chamber is the same as the pressure in the driver chambers, minimizing the difference in pressure across each driver diaphragm. Communication between all chambers is via a vent line. The system is also capable of being placed under a vacuum to degas the fluid in the sample and remove bubbles acquired while filling the sample cavity. O-rings are used to seal the chamber against leakage of gas from the driver side and leakage of liquid from the sample side. Samples are enclosed in a copper sleeve for easy installation and removal. The sleeve is three inches long and has an inner diameter of 1.50 inches and an outer diameter of 1.66 inches.

2. Fluid Management System

Figure 18 represents the fluid system used to support coupler operation. A description of fluid system operation is given below.

To fill the chamber, the pressure source (pressurized nitrogen gas) is isolated. The chamber and the reservoir are then exposed to a vacuum. The chamber and fluid are evacuated to degas as much as possible. The fluid reservoir is then isolated from the vacuum on the main vent side. The main vent valve is then cracked open. The fluid is driven by atmospheric pressure into the sample chamber.

The vent line on the chamber is constructed of high pressure nylon braided tubing. A fluid level is established at the lower portion of this tubing, just above the connection to the chamber. The main

41

vent valve is shut, and the reservoir is again exposed to vacuum. The level in the chamber vent line may lower out of sight, so the fill procedure is repeated until the level remains visible in the tubing.

Once a fluid level is established, the chamber is isolated from the vacuum and reservoir. The valve to the pressure source is opened and pressure is slowly brought up to two atmospheres. Pressure is held there for 30 minutes. This ensures that any remaining gases are forced back into solution. The liquids to be used in this experiment
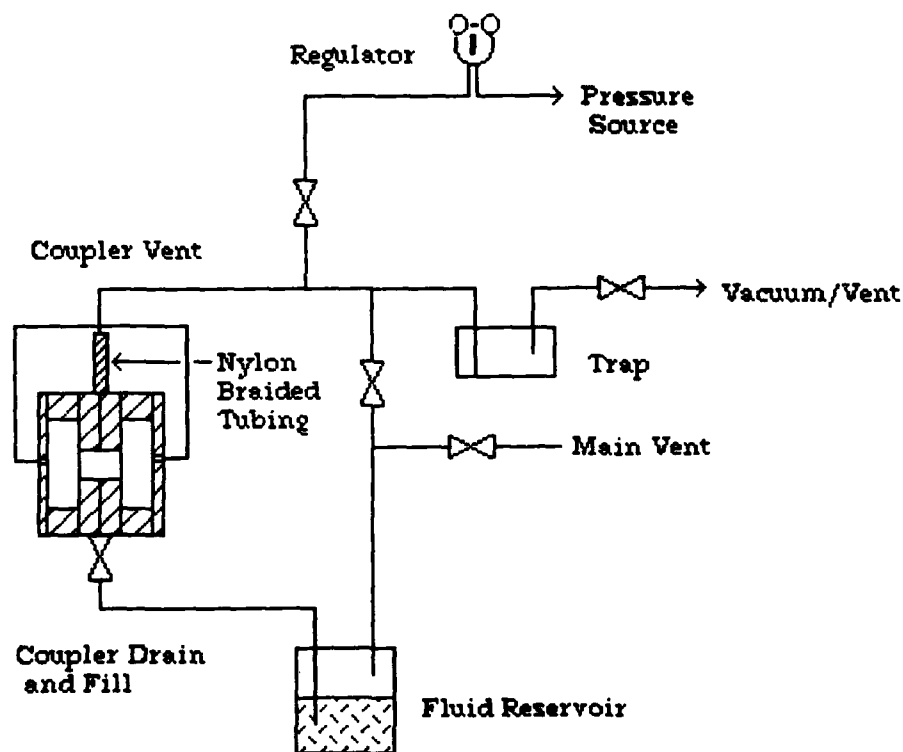

Figure 18. Fluid System.

are Fluorinert liquids. These fluids are manufactured by the 3M Company [Ref. 16]. This type of fluid has been used successfully in similar experiments.

IV. PRELIMINARY EXPERIMENTS AND RESULTS

A. INTRODUCTION

Several preliminary experiments were preformed to validate the concept that the acoustic load presented to the face of each driver, particularly a moving mass, can be extracted from its input electrical impedance. Experiments were performed with a water-filled tube open in air, with the empty coupler and with the coupler filled with water. One important result of these preliminary experiments was the need to include a correction factor for the difference in the cross-sectional area of the sample chamber and the driver diaphragm.

B. WATER-FILLED TUBE

1. Description of Tube

Once we had confidence in our ability to characterize the driver, an experiment was conducted with a water-filled tube placed over the driver to see if the mass of water added could be extracted from its input electrical impedance. A driver was fitted with a special water-tight cover plate with tube, as shown in Figure 19. The tube and cover were machined to the exact diameter of the diaphragm, including surround.

2. Resonance Experiment

A known volume of water was added to the tube, and the shift in resonance frequency was recorded. Table 4.1 lists the resonance frequencies for the volume of water added. The lowering of the

44

resonance with mass added is expected. These values will be quantitatively analyzed further to determine if the resonance
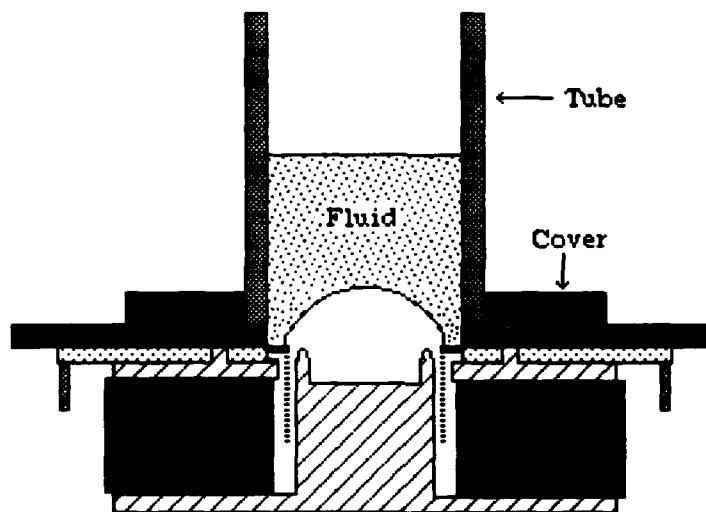

Figure 19. Initial Test Apparatus.

frequency shift is that expected, i.e., does the resonance frequency shift predict the correct mass added?

TABLE 4.1. RES. FREQUENCY FOR ADDED WATER.	
Volume Added (ml)	Res. Frequency (Hz)
0.0	1000
5.0	319
10.0	226
15.0	188
20.0	160

3. Cross-Sectional Area Correction Factor

The resonance frequency data were reduced by comparing the results of the observed resonance frequency with a predicted value. A ratio of Equation 3.8 and 3.9 was established, and from the known stiffness and mass of the driver, the added mass was determined.

45

When the calculated masses were compared to the masses added, they were half of the expected value for all volumes added.

The data were analyzed in another manner by plotting the period squared versus the mass added and is shown in Figure 20. As discussed in Section III.B.3.c., the ratio of intercept to slope yields
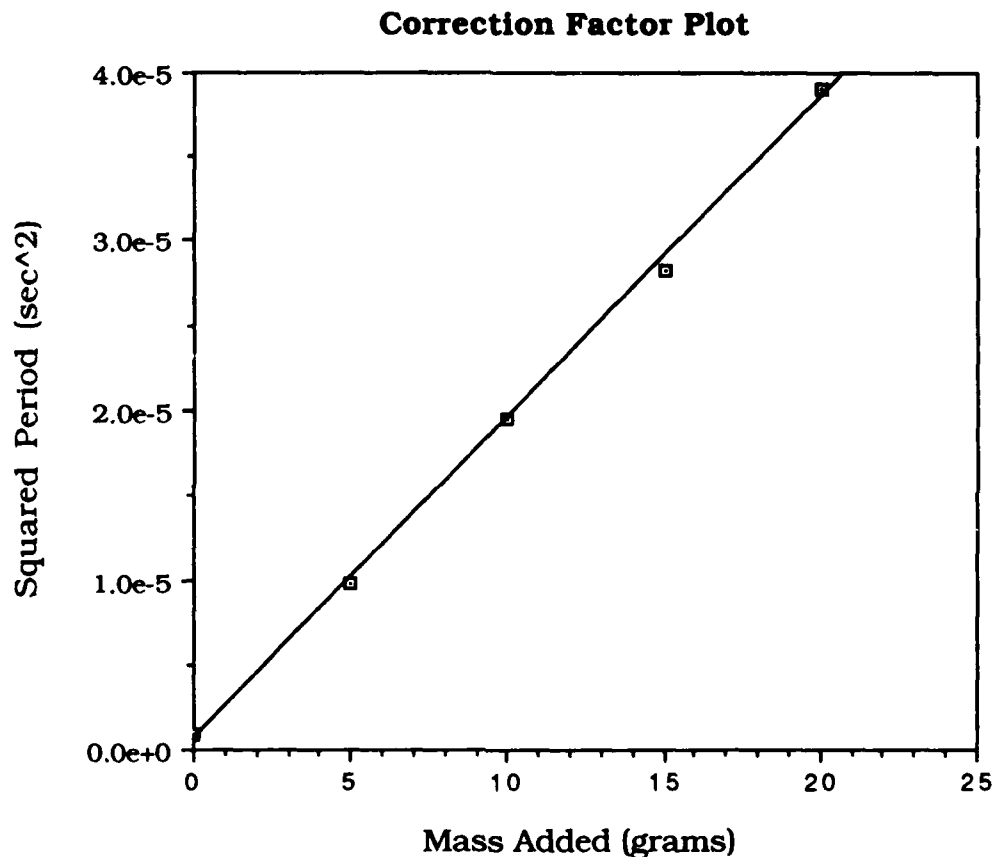
Correction Factor Plot

Figure 20. Correction Factor Data

the mass of the driver. When this was accomplished, the calculated moving mass was double the known value.

This apparent discrepancy in the results can be understood as follows. It was assumed the driver acts as a piston with uniform

46

displacement across the width of the tube for a specific current and frequency. In reality, the edges of the speaker are fixed so this assumption is crude at best.

A better approximation of the driver displacement profile is that shown in Figure 21. The displacement is assumed to increase
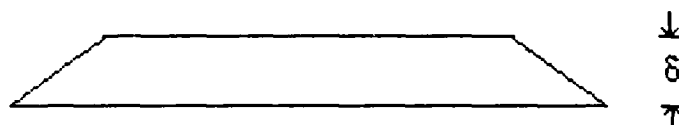

Figure 21. Assumed Diaphragm Displacement.

linearly across the surround and then stay constant across the dome. Using this profile, the ratio of the average velocity of the fluid above the driver was compared to the velocity of the voice coil, which is attached to the dome. The kinetic energy of the water added was set equal to the kinetic energy imparted by the voice coil. Referred to the voice coil, the effective mass of water added is given by:

$$m_e = \frac{2\ KE}{v_{vc}^2} ,$$

(4.2)

where KE is the kinetic energy of the energy of the water, and v_{vc} is the velocity of the voice coil. The ratio of m_e to m_{water} depends only on the diameters of the tube and diaphragm and the diaphragm velocity profile. We call this ratio the "area correction factor" since it is essentially the square of the ratio of the tube cross-sectional area to the cross-sectional area of the dome. The resulting ratio for the

47

velocity profile in Figure 21 is:

$$\frac{m_e}{m_{water}} = 0.71 \ .$$ (4.3)

In other words, provided the displacement profile is the one assumed, the effective mass of the water presented to the transducer is only 0.71 times the actual mass of water added. Since the actual profile of the transducer displacement is not really known, the observed value of 0.5 obtained from the resonance experiments can be considered a "calibration" value of m_e/m_{water} for the tube. A similar calibration will be needed for the drivers in the coupler.

4. Broad Band Experiment

Once the area correction factor for the tube was obtained, experiments were conducted in an attempt to extract the radiation impedance ($\tilde{Z}_r$) presented to the diver over as broad a frequency range as possible (hopefully 100-1000 Hz). Referring to Figure 8, the procedure is to obtain the electrical input impedance of the driver and the tube with no added fluid (with single driver operation, the current is no longer halved). Assuming negligible air loading, this can be considered as the series impedance of $\tilde{Z}_E + \tilde{Z}_M$. The blocked electrical impedance ($\tilde{Z}_E$) is subtracted from the input electrical impedance and the results are stored in the HP-4194A. The result is the electrical equivalent mechanical impedance, $\tilde{Z}_M$.

Fluid is now added to the tube and the procedure repeated. The result is the parallel combination of $\tilde{Z}_M$ and $\tilde{Z}_R$. Since $\tilde{Z}_M$ is

48

known, $\tilde{Z}_R$ can be solved for (Section II.D.) using register manipulation on the HP-4194A. $\tilde{Z}_r$ is then obtained from:

$$\tilde{Z}_r = \frac{(Bl)^2}{\tilde{Z}_R} .$$

(4.4)

The real part of $\tilde{Z}_r$ is the radiation resistance, while the imaginary part is the radiation reactance.

For the case of fluid in the tube above the voice coil, the magnitude of the radiation reactance is equal to ωM_e where ω is the angular frequency and M_e is the effective mass added. The HP-4194A has the ability to perform the scalar multiplication required to extract the added mass. This mass value can be compared to the mass added to evaluate the effectiveness of detecting the added mass using the acoustically "soft" transducers selected.

Using the area correction factor mentioned earlier, the values of measured mass versus actual mass agreed to within five per cent of each other over 80 per cent of the frequency span between 100 to 1000 Hz. Over the remaining 20 per cent of the span differences larger than five per cent can be attributed to the tube resonances that occur in the air in the unfilled portion of the tube. These should be eliminated when the chamber is tested full of liquid.

C. COUPLER EXPERIMENTS

1. Repeat of Water Filled Tube Experiments With Half of Coupler

Since the area of the sample chamber is greater than the area of the tube used earlier, a new area correction factor for the drivers installed in the coupler must be obtained.

a. Resonance Shift

The initial experiment conducted with the chamber was to establish an area correction factor for each driver, as described in Sections IV.B.2 and IV.B.3. Only one driver is tested at a time, with the driver and the chamber placed in the vertical position. Water is added to the open end of the chamber. Several different volumes of water are added and the resonance frequency recorded for each. The frequencies and added volumes are listed in Table 4.2. With 50 ml of water added, the water level was high enough to reach the vent holes in the sample sleeving. Double this volume is a good estimate of the chamber volume with both drivers attached.

TABLE 4.2. CHAMBER CALIBRATION	
Volume added (ml)	Resonance Frequency (Hz)
0.0	944.1
10.0	266.1
15.0	221.3
20.0	190.5
25.0	171.8
30.0	156.7
35.0	146.2
40.0	138.0
45.0	130.3
50.0	123.0
70.0	104.7

b. Area Correction Factor

The data in Table 4.2 were reduced for the effective mass added as described in Section IV.B.3. An area correction factor was determined for each driver based upon the reduced data. The average of the two area correction factors, to be used in further testing, is 0.3108. The area correction factors for the two different drivers agreed to within four per cent, reconfirming the similarity of the two drivers.

c. Broad Band Experiments

Once an area correction factor was determined, broad band measurements of input electrical impedance were made for added water volumes of 10, 20, and 50 ml. Applying the procedure mentioned in Section IV.B.4, the data were reduced, resulting in extracted radiation mass as a function of frequency. Figure 22 is an example of the results obtained for 10 ml of added water. For all three added volumes, the extracted values of mass versus added frequency were within 10 per cent of the actual value. Over most of the frequency band, the data was within five per cent of the correct mass.

2. Experiments With Complete Coupler

a. Air Filled

Prior to conducting a test of the chamber filled with water, it was first operated with only air in the chamber. Both modes of operation were tested: the in-phase "push-push" mode, and the out-of-phase "push-pull" mode. The resulting plots of impedance

magnitude versus frequency are shown for the two cases in Figures 23 and 24, respectively.

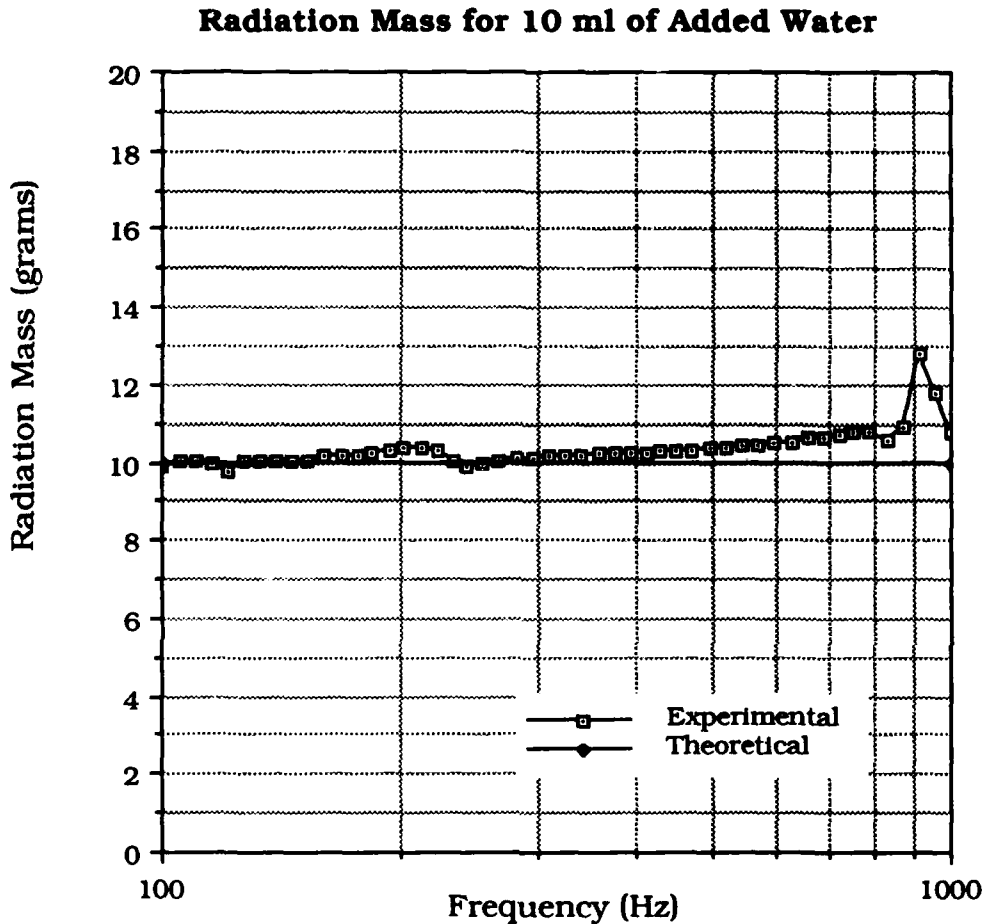**Radiation Mass for 10 ml of Added Water**

Figure 22. Mass Extracted from Impedance for 10 ml of Added Water.

An analysis of the data reveals resonances of the air in the chamber. The push-push data showed resonances at frequencies for which the chamber length was an integral multiple of the wavelength. The push-pull mode exhibited resonances when the chamber length was an odd half-integer multiple of the wavelength. Also, these figures

52

demonstrate the drivers do indeed appear electrically as one driver with half the impedance, when operated in parallel. Since the results
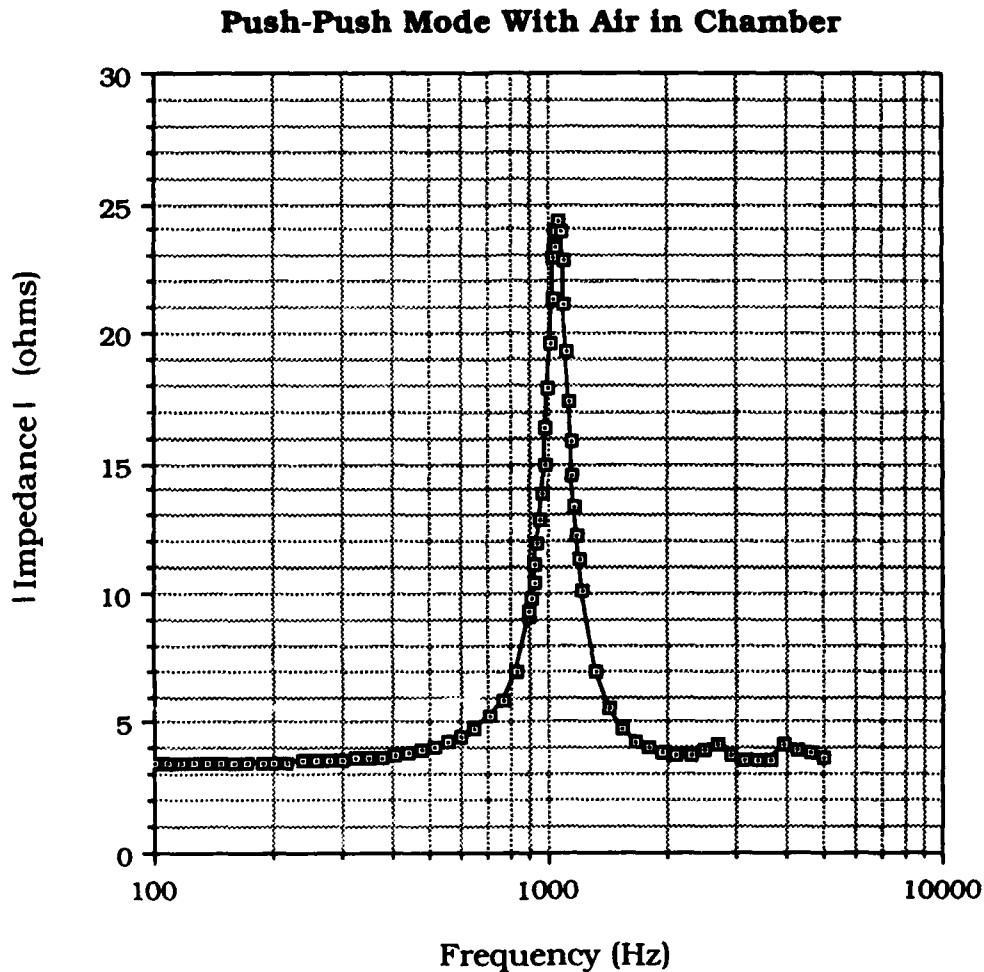

Figure 23. Push-Push Operation for Air Only.

were favorable for the air-only case, the final experiment performed was to fill the chamber with degassed water and from the measured input electrical impedance of the drivers wired in parallel out-of-phase, extract the mass of the water.
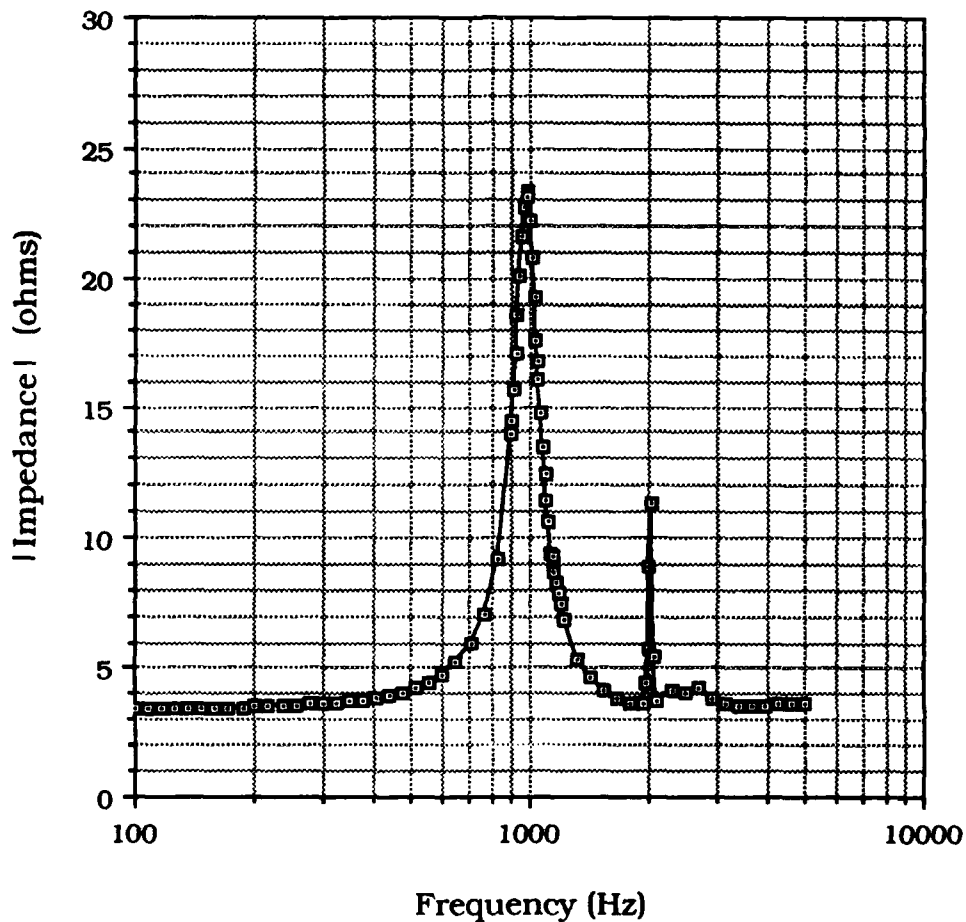
53

Push-Pull Mode With Air in Chamber

Figure 24   Push-Pull Operation for Air Only.

b. Water Filled

With the chamber filled with water, the HP-4194A was used to measure the input electrical impedance (as a function of frequency) of the drivers wired in parallel out-of-phase. The acoustic radiation impedance $\tilde{Z}_R$ was obtained as described in Section IV.B.4. $\tilde{Z}_R$ was

54

further reduced to obtain the radiation mass of the water as described in Section II.D.

The results are shown in Figure 25. The expected value of radiation mass was 50 grams. The agreement is poor. At about 200 Hz, there is evidence of an unexpected resonance in the system. A preliminary analysis of the system leads us to believe this is a
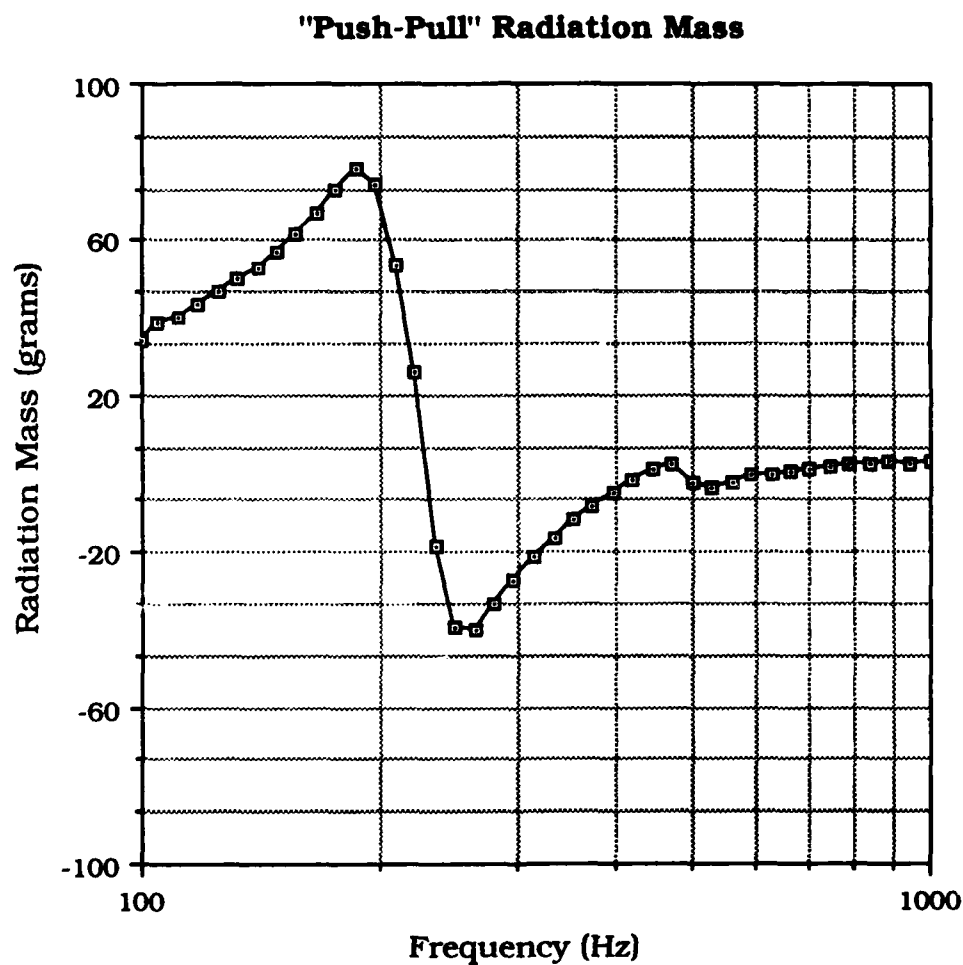
"Push-Pull" Radiation Mass

Figure 25. Radiation Mass of Fluid Filled Coupler.

55

resonance of the mass of fluid in the vent hole and the spring of the air in the tubing above it. It is expected that this unwanted resonance can be eliminated by installing a valve in the vent hole which can be closed after filling with fluid.

V. CONCLUSIONS AND RECOMMENDATIONS

A method has been described by which the complex bulk modulus $\tilde{B}$ and complex effective mass density $\tilde{\rho}$ for a fluid contained in a rigid porous solid can be extracted from measured input electrical impedance of a pair of identical transducers wired in parallel in-phase and out-of-phase.

A pair of moving coil transducers was selected and their electromechanical performance was characterized.

A cylindrical brass coupler chamber was designed and built.

Several preliminary experiments were conducted to verify the ability to extract the density from measured input electrical impedance. The results for the most part were accurate to within five per cent of expected values. The only measurements that exceeded this limit were those taken during preliminary parallel driver operation for the water filled chamber. Complete characterization of the fluid filled chamber still remains to be done.

Other areas for future research include adding a valve to the vent line, repeating the water filled experiment, then interpret the results for both push-pull and push-push operation. Once system operation has been verified with water, $\tilde{B}$ and $\tilde{\rho}$ of simple rigid porous solids can be obtained, providing additional validation of the theory prior to the testing of the more complex porous solids.

APPENDIX

FLUID FILLED POROUS MEDIA EFFECTS

This appendix presents a discussion of the effect of placing a fluid in a rigid porous solid on its density, bulk modulus and speed of sound. Derivations for a simple bulk fluid are followed by those for a fluid-filled porous solid. The frame of the porous solid is assumed to be rigid. The losses in the fluid saturated porous solid are assumed to be associated with the shear viscosity of the fluid.

The continuity equation for a bulk fluid is [Ref. 17:pp. 106-108]:

$$\frac{\partial \rho}{\partial t} + \nabla \left(\rho \vec{u} \right) = 0. \tag{A.1}$$

For a fluid contained in a rigid porous solid, this formula becomes

$$\frac{\partial \langle \rho \rangle}{\partial t} + \nabla \left(\langle \rho \vec{u} \rangle \right) = 0, \tag{A.2}$$

where,

$\langle \rho \rangle$ = the spatial average of the microscopic fluid mass density.

$\langle \rho \vec{u} \rangle$ = the spatial average of the microscopic fluid momentum density.

Assuming a one dimensional, time harmonic solution to these equations, they become in linearized form:

$$j\omega\rho + \rho_0 \frac{\partial \tilde{u}}{\partial x} = 0, \tag{A.3}$$

$$j\omega\langle\rho\rangle + \rho_0 \frac{\partial \langle \widetilde{u} \rangle}{\partial x} = 0. \tag{A.4}$$

58

Now consider Newton's second law for a fluid [Ref. 17:pp. 111-115]:

$$\rho \frac{\partial \vec{\tilde{u}}}{\partial t} + \left(\vec{\tilde{u}} \cdot \nabla \right) \vec{\tilde{u}} = -\nabla \tilde{p} + \eta \nabla \times \nabla \times \vec{\tilde{u}} . \qquad (A.5)$$

Assuming a one dimensional, time harmonic solution and neglecting viscosity for the bulk fluid, this becomes in linearized form,

$$j\omega \rho_0 \tilde{u} = -\frac{\partial \tilde{p}}{\partial x} . \qquad (A.6)$$

The corresponding equation for a fluid-saturated porous solid, including viscosity is:

$$j\omega \rho_{eff} \langle \tilde{u} \rangle = -\frac{\partial \langle \tilde{p} \rangle}{\partial x} - R_{flow} \langle \tilde{u} \rangle , \qquad (A.7)$$

where

ρ_{eff} = the effective fluid mass density,

$\langle \tilde{u} \rangle$ = the spatial average of the microscopic fluid velocity,

$\langle \tilde{p} \rangle$ = the spatial average of the microscopic pressure,

R_{flow} = the flow resistance.

ρ_{eff} and R_{flow} are operationally defined by:

$$\frac{1}{2}\rho_{eff} \langle \tilde{u} \rangle^2 = \text{kinetic energy density within the fluid, and}$$

$$\langle \tilde{u} \rangle^2 R_{flow} = \text{rate of decay of fluid kinetic energy density} \\ \text{due to shear viscosity.}$$

In general, $\rho_{eff} \geq \rho$. Also, for steady flow, $R_{flow} \equiv R_{DC}$ and

$$R_{DC} \propto \frac{\eta}{(\text{pore size})^2} , \qquad (A.7a)$$

where η is the fluid shear viscosity.

It is convenient to combine the velocity terms in Equation A.7 and define the complex fluid mass density, $\tilde{\rho}$, by:

$$j\omega \langle \tilde{u} \rangle \tilde{\rho} = - \frac{\partial \langle \tilde{p} \rangle}{\partial x} . \qquad (A.8)$$

Hence

$$\tilde{\rho} = \rho_{eff} + \frac{R_{flow}}{j\omega} . \qquad (A.9)$$

To develop a wave equation, first the time derivative of the continuity equation is subtracted from the spatial derivative of Newton's second law. Applying this to the bulk fluid case,

$$\omega^2 \rho = \frac{\partial^2 \tilde{p}}{\partial x^2} . \qquad (A.10)$$

For the porous solid, the corresponding equation is:

$$-\omega^2 \frac{\tilde{\rho}}{\rho_0} \langle \rho \rangle = \frac{\partial^2 \langle \tilde{p} \rangle}{\partial x^2} . \qquad (A.11)$$

The next step is to momentarily examine the bulk modulus. The definition of bulk modulus is [Ref. 18]:

$$B \equiv \rho_0 \left(\frac{\partial \tilde{p}}{\partial \rho} \right) . \qquad (A.12)$$

For the fluid in the porous solid the corresponding definition is:

$$\tilde{B} \equiv \rho_0 \left(\frac{\partial \langle \tilde{p} \rangle}{\partial \langle \rho \rangle} \right) . \qquad (A.13)$$

Substituting these expressions into Equations A.10 and A.11, the following results:

$$-\omega^2 \rho = \frac{B}{\rho_0} \frac{\partial^2 \tilde{\rho}}{\partial x^2} , \qquad (A.14)$$

for the bulk fluid, and

$$-\omega^2 \langle \rho \rangle = \frac{\tilde{B}}{\tilde{\rho}} \frac{\partial^2 \langle \rho \rangle}{\partial x^2} , \qquad (A.15)$$

for the fluid saturated porous solid.

Equation A.14 is the usual wave equation for the propagation of sound in a bulk fluid, with a wave speed given by:

$$c^2 = \frac{B}{\rho} . \qquad (A.16)$$

Equation A.15 is the wave equation for the propagation of sound in a fluid-saturated, rigid porous solid, with a wave speed given by:

$$\tilde{c}^2 = \frac{\tilde{B}}{\tilde{\rho}} . \qquad (A.17)$$

Hence the speed of sound in a fluid saturated, rigid porous solid is a complex quantity which is obtained from the complex bulk modulus and complex fluid mass densities in exactly the same way the speed of sound in a bulk fluid is obtained from the bulk modulus and fluid mass density.

REFERENCES

1. Biot, M. A., "Theory of Propagation of Elastic Waves in Fluid Saturated Porous Solids: I. Low Frequency Range," Journal of the Acoustical Society of America, v. 28, p 168, 1956.

2. Biot, M. A., "Theory of Propagation of Elastic Waves in Fluid Saturated Porous Solids: II. High Frequency Range," Journal of the Acoustical Society of America, v. 28, p 179, 1956.

3. Stoll, R. D., "Acoustic Waves in Saturated Sediment," Physics of Sound in Marine Sediment, p. 19, 1974.

4. Ogushwitz, P. R., "Applicability of the Biot Theory: I. Low Porosity Materials," Journal of the Acoustical Society of America, v. 77, p.429, 1985.

5. Stoll, R. D., "Marine Sediment Acoustics," Journal of the Acoustical Society of America, v. 77, p. 1789, 1985.

6. Baker, S. R., Sound Propagation in a Superfluid Helium Filled Porous Solid: Theory and Experiment, PhD Dissertation, Department of Physics, University of California at Los Angeles, 1986.

7. Kinsler, L. E., and others, Fundamentals of Acoustics, 3rd ed., John Wiley & Sons, Inc., 1982.

8. Wilson, O. B., An Introduction to the Theory and Design of Sonar Transducers, p. 23, U. S. Government Printing Office, 1985.

9. Hall, D. E., Basic Acoustics, pp.265-267, Harper and Row, 1959.

10. Morse, P. M., Vibration and Sound, 2nd ed., pp. 233-237, McGraw-Hill Book Company, 1948.

11. Hofler, T., Private Communication, Physics Department, Naval Postgraduate School, Monterey, CA, 1988.

12. Apollo Electronics, Santa Monica, CA.

13. Hewlett-Packard Corporation, San Jose, CA.

14. G. L. Collins Corporation, Long Beach, CA.

15. Stanford Research System, Stanford, CA.

16. Minnesota Mining and Manufacturing (3M), St. Paul, MN.

17. Daily, J. W., and others, Fluid Dynamics, Addison-Wesley Publishing Company, 1973.

18. Morse, P. M. and Ingard, K. U., Theoretical Acoustics, pp. 228-230, McGraw-Hill Book Company, 1956.

INITIAL DISTRIBUTION LIST

		No. Copies
1.	Defense Technical Information Center Cameron Station Alexandria, VA 22304-6145	2
2.	Library, Code 0142 Naval Postgraduate School Monterey, CA 93943-5002	2
3.	Professor O. B. Wilson (Code 61Wl) Naval Postgraduate School Monterey, CA 93943-5000	2
4.	Professor S. R. Baker (Code 61Ba) Naval Postgraduate School Monterey, CA 93943-5000	8
5.	Dr. Pieter S. Dubbleday Naval Research Laboratory Underwater Sound Reference Detachment Orlando, FL 32856	2
6.	Professor S. L. Garrett (Code 61 Gx) Naval Postgraduate School Monterey, CA 93943-5000	1
7.	LT S. D. Grant Box 193 Lander, WY 82520	1
8.	Officer-in-Charge Attention: Code 9032 Naval Undersea Warfare Engineering Station Hawaii Detachment Lualualei, HI 96792	1
9.	Dr. R. Y. Ting Naval Research Laboratory Underwater Sound Reference Detachment Orlando, FL 32856	1

10. Dr. B. Tittman   1
  Rockwell Science Center
  Camino Dos Rios
  Thousand Oaks, CA 91360

11. Dr. E. L. Hamilton   1
  Code 541 (T), Bldg. 305
  Naval Ocean System Center
  San Diego, CA 92152